

Channel Estimation in Wireless OFDM Systems: Interpolation versus ESPRIT

A Thesis

Presented to

the faculty of the School of Engineering and Applied Science

University of Virginia

in partial fulfillment
of the requirements for the degree

Master of Science

by

Mrugen Anil Deshmukh

May 2018

APPROVAL SHEET

This Thesis
is submitted in partial fulfillment of the requirements
for the degree of
Master of Science

Author Signature: 

This Thesis has been read and approved by the examining committee:

Advisor: Prof. Stephen G. Wilson

Committee Member: Prof. Maite Brandt-Pearce

Committee Member: Prof. Farzad Farnoud

Committee Member: Dr. Satya Prakash Ponnaluri

Committee Member: _____

Committee Member: _____

Accepted for the School of Engineering and Applied Science:



Craig H. Benson, School of Engineering and Applied Science

May 2018

Foreword

This research was supported by a project funded by the National Spectrum Consortium, aimed at improving data rates within congested spectrum on Air Force telemetry ranges. The adopted technical approach is a multi-channel OFDM physical-layer with channels chosen to avoid legacy users in the upper C-band range (around 6 GHz). Each OFDM channel uses a 128-point FFT design, with 100 active subcarriers. Spacing between channel centers is assumed to be 2 MHz.

The current thesis centers on channel identification for performing frequency-domain equalization, one of the primary attractions of OFDM. Most of the development is generic (beyond this project), though simulations and parameter choices have followed those of the project design.

Stephen G. Wilson

*This thesis is dedicated to my parents,
Swati and Anil.*

Abstract

With the rapid growth of digital communication in recent years, the need for high speed data transmission is increased. Moreover, future wireless systems are expected to support a wide range of services which includes video, data and voice. OFDM is a widely standardized candidate for achieving high data rates in mobile environment, due to its resistance to ISI, which is a common problem found in high speed data communication.

In OFDM systems, estimating channel frequency response is essential to successful data recovery. In this thesis, traditional estimation methods using interpolation among pilot measurements are compared to a parametric model (PM)-based channel estimation. This PM-based technique uses the ESPRIT (Estimation of Signal Parameters by Rotational Invariance Techniques) method to estimate time delays of multiple paths in the channel. Then a least-squares estimator is used to estimate the channel frequency response. Performance of these techniques in terms of symbol error rate and time-complexity is compared. Though this subspace method is computationally more expensive, experimental results show that it performs much better than traditional interpolation techniques.

Use of LDPC channel coding to reduce bit error rates in frequency-selective channels is also explored.

Acknowledgements

I would like to first thank my advisor, Prof. Stephen G. Wilson for giving me an opportunity to do research with him.

I would like to thank my committee members, Prof. Maite Brandt-Pearce, Prof. Farzad Farnoud, and Dr. Satya Prakash Ponnaluri for devoting their time to be on my thesis committee.

I would also like to thank Marc Severo for helping me settle into this project, and Rui Shang and Ruixuan He for all their research contributions.

I am grateful to everyone at University of Virginia who have taught or supervised me, and to Beth Eastwood-Beatty for helping me throughout the program.

Last but not least, I would like to thank my parents, Swati and Anil Deshmukh for their constant support and encouragement.

Contents

Foreword	iii
Abstract	v
Acknowledgements	vi
List of Figures	ix
List of Tables	xi
Glossary of Terms	2
1 Introduction	4
1.1 Contribution	5
1.2 Organization of thesis	6
2 OFDM basics	7
2.1 OFDM System Overview	8
2.2 OFDM channel modulation	11
2.3 OFDM channel demodulation	12
3 Wireless transmission channel	14
3.1 Channel model	15
3.1.1 Frequency-selective channels	17
3.1.2 Time-selective channels	17

3.2	Frequency response in multipath channels	18
3.3	Other propagation characteristics	22
3.3.1	Noise	22
3.3.2	Frequency offset	23
4	Channel estimation	25
4.1	CFR-based estimation	27
4.1.1	Linear interpolation	29
4.1.2	Cubic spline interpolation	30
4.2	PM-based estimation	31
5	Simulation and results	36
5.1	Results	36
5.1.1	Effect of delay spread on the channel and estimation	37
5.1.2	M-ary QAM constellations	38
5.1.3	Symbol error rate	44
5.1.4	Shortcomings of ESPRIT-based algorithm	46
6	Channel coding	48
6.1	Motivation	48
6.2	Introduction to channel coding	49
6.3	LDPC codes	53
6.3.1	LDPC encoding	55
6.3.2	LDPC decoding	55
6.4	Simulation results	58
7	Conclusion	61
8	Bibliography	63

List of Figures

2.1	OFDM Subcarriers	8
2.2	OFDM system block diagram	10
2.3	Cyclic prefix in an OFDM symbol	10
2.4	OFDM modulation block diagram	12
2.5	OFDM demodulation block diagram	13
3.1	Two-path propagation model	15
3.2	Impulse response model for a frequency-selective channel	18
3.3	Impulse response model for a time-selective channel	19
3.4	Ideal channel frequency response	20
3.5	Two-path channel frequency response	21
3.6	Four-path channel frequency response	22
4.1	Schemes for loading pilot symbols in OFDM	28
4.2	Linear interpolation between pilots of a 2-path channel in (4.4)	30
4.3	Cubic spline interpolation between pilots of a 2-path channel in (4.4)	31
4.4	ESPRIT estimation for pilots of a 2-path channel in (4.4)	34
5.1	Effect of changing delay spread	39
5.2	Effect of increasing the delay spread on the probability of error ($E_b/N_0 =$ 60 dB, linear interpolation)	40
5.3	Constellations for 16-QAM	41
5.4	Constellations for QPSK	42

5.5	Symbol error rate plots for ideal channel	44
5.6	Symbol error rate plots for the two-path channel	45
5.7	Symbol error rate plots for the three-path channel	46
5.8	Constellations for a delay spread of $7\mu s$	47
6.1	Error distribution within OFDM symbols in a 2 path channel with noise.	49
6.2	Block diagram of a basic digital communication system	50
6.3	Graph representation of LDPC code in (6.4)	55
6.4	BER plot for AWGN channel, $R = 0.84$, $(N, K) = (6400, 5376)$	59
6.5	BER plot for two-path channel, $R = 0.84$, $(N, K) = (6400, 5376)$	60

List of Tables

5.1	System Parameters	37
5.2	RMSE and time required for channel estimation	43

Glossary of Terms

ADC	Analog-to-Digital Converter.
ASAM	Adaptive Spectrum Aggregation & Management.
AWGN	Additive White Gaussian Noise.
CFR	Channel Frequency Response.
CIC	Cascaded Integrator Comb.
CN	Check Node.
CP	Cyclic Prefix.
DAC	Digital-to-Analog Converter.
DFT	Discrete Fourier Transform.
DSP	Digital Signal Processing.
FCC	Federal Communications Commission.
FDE	Frequency Domain Equalizer.
FDM	Frequency Division Multiplexing.
FDMA	Frequency Division Multiple Access.
FEC	Forward Error Correction.
FFT	Fast Fourier Transform.
FIR	Finite Impulse Response.
FPGA	Field-Programmable Gate Array.
ICE	Iterative Channel Estimation.
IDFT	Inverse Discrete Fourier Transform.

IFFT	Inverse Fast Fourier Transform.
ISI	Inter-Symbol Interference.
LDPC	Low Density Parity Check.
LNA	Low Noise Amplifier.
LTE	Long-Term Evolution.
MIMO	Multiple-Input Multiple-Output.
OFDM	Orthogonal Frequency Division Multiplexing.
OFDMA	Orthogonal Frequency Division Multiple Access.
PAPR	Peak to Average Power Ratio.
PSF	Pulse Shaping Filter.
QAM	Quadrature Amplitude Modulation.
QPSK	Quadrature Phase Shift Keying.
RF	Radio Frequency.
RMSE	Root Mean Square Error.
RRC	Root Raised Cosine.
SER	Symbol Error Rate.
SNR	Signal-to-Noise Ratio.
T&E	Test & Evaluation.
VN	Variable Node.

Chapter 1

Introduction

Due to the increasing demand on bandwidth in the RF spectrum, Orthogonal Frequency Division Multiplexing (OFDM) has been a popular physical layer multicarrier access strategy in wireless communication systems. OFDM appears in standards such as 802.11a/g/n/ac, LTE, satellite audio broadcasting, DVB-T, etc.

OFDM is a digital multi-carrier modulation scheme, which uses a large number of closely-spaced orthogonal sub-carriers that is particularly suitable for frequency-selective channels and high data rates. This technique transforms a frequency-selective wide-band channel into a group of non-selective narrow-band channels, which makes it robust against large delay spreads by preserving orthogonality in the frequency domain. This also leads to high spectral efficiency, ability to equalize highly dispersive channel in the frequency domain and simplified transceiver structure [1].

Enabled by the use of cyclic prefix, which will be discuss later in the thesis, equalization at the receiver is simple in OFDM systems. The simplified equalization at receiver, however, requires knowledge of the channel over which the signal is transmitted. In a wireless communication channel, the transmitted signal goes through degradation during propagation. This degradation may be attributed mainly to noise and multipath fading.

To facilitate the estimation of the channel in an OFDM system, known signals or pilots are typically inserted in the transmitted OFDM symbol. Different methods can then be applied to estimate the channel using these known pilots [2].

The main objective of this thesis is to investigate and compare two competing approaches for pilot-aided channel estimation: interpolation among received pilot measurements, and use of a subspace method which identifies multipath channel impulse response, based on ESPRIT. This comparison is done by examining the quality of channel frequency response estimates, the impact on signal constellations after equalization, and symbol error probability (SEP) for QPSK and 16-QAM modulation. Use of Low Density Parity Check (LDPC) codes to improve the SEP performance of the OFDM system is also investigated.

1.1 Contribution

The main contribution of this thesis is to compare traditional pilot-based interpolation techniques (linear and cubic spline) used to estimate channel frequency response in a slow-fading frequency selective wireless channel to a parametric model-based technique. This comparison is made in terms of the time complexity of each technique and performance of the techniques in symbol error probabilities. A root-mean-square error metric is also defined to check the accuracy of each technique in estimating the channel frequency response. A technical paper about the same is published in the proceedings of *2018 IEEE 8th Annual Computing and Communication Workshop and Conference (CCWC)* [3].

1.2 Organization of thesis

Chapter 2 contains background of OFDM, the OFDM baseband model used in simulations and top-level description of an OFDM system.

Chapter 3 focuses on wireless transmission channels. The propagation effects a signal goes through in a wireless channel are described here. Mathematical model of the channel is defined and effects of multipath fading on the channel frequency response are detailed.

Chapter 4 focuses on channel estimation. Broad overview of existing channel estimation techniques is provided. Channel estimation techniques used in simulations are described in detail.

Chapter 5 describes the experimental setup used in simulations and demonstrates results. It displays and compares the performance of channel estimation techniques with respect to RMSE values between true CFR and estimated CFR, time complexity and symbol error rate plots in the presence of noise and delay spread (multipath fading).

Chapter 6 is dedicated to channel coding. It explains the motivation to use channel coding, introduces existing channel coding techniques and lastly focuses on the LDPC encoding/decoding used in simulations.

Chapter 7 Summarizes the experiments and results presented in the thesis and discusses possible future work.

Chapter 2

OFDM basics

Orthogonal frequency division multiplexing (OFDM) has lately been the most popular choice of modulation scheme in next-generation wireless communication systems. A primary attribute of OFDM is simple channel equalization in the frequency domain due to its block based transmission scheme. OFDM transforms a large-bandwidth, frequency-selective multipath fading channel into multiple orthogonal narrow-bandwidth flat fading channels. In addition to low-complexity equalization, this channel separation also allows for frequency-domain bit loading and simple orthogonal user allocation.

In OFDM, Quadrature Amplitude Modulation (QAM) subcarriers are spaced on the interval of the reciprocal of symbol duration, $1/T$ [1]. This subcarrier spacing is defined to be Δ . The spectrum of this is the sum of overlapping *sinc()* functions with null-to-null bandwidth of 2Δ for each subcarrier. As can be seen in Figure 2.1, subcarriers do overlap, but are orthogonal to each other and their interference is cancelled out at the subcarrier spacing. This is an assumption for ideal OFDM channels. Figure 2.1 shows how dense packing of subcarriers helps save bandwidth which would have been used up by a predecessor of OFDM (such as FDMA).

Dense channel packing with sub-carriers also allows for efficient channel estimation in the

frequency domain, which shall be discussed later in this thesis. Another key advantage of OFDM is that the modulation structure can allow multiple users to utilize different subcarriers in the same spectrum.

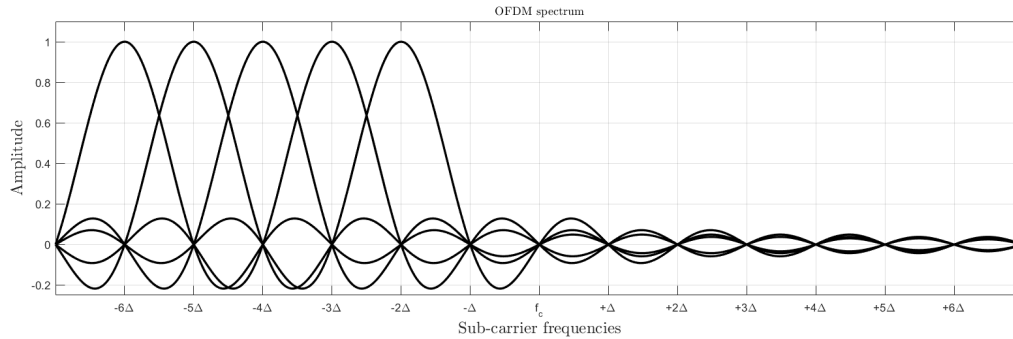


Figure 2.1: OFDM Subcarriers

OFDM does have its drawbacks. OFDM symbols are susceptible to frequency offsets, failure to compensate for which will lead to bad equalization. There may be large instantaneous power fluctuations in an OFDM symbol over its symbol period (T) which can be difficult for the power amplifiers at the transmitter to reproduce without distortion. Another drawback is that timing estimation can be more complicated in OFDM than in single-carrier transmission systems. A viable alternative to avoid the drawbacks of OFDM could be single-carrier QAM (e.g. adaptive linear equalizer). Channel estimation and equalization in single-carrier QAM however, is more complicated than in OFDM and is out of scope of this thesis.

2.1 OFDM System Overview

Consider an OFDM system with N subcarriers. Among these, $N_d + 1$ sub-carriers in the center of the spectrum are used to transmit data. In wireless channels, linear distortions such as multipath fading may cause sub-carriers at the edge to interfere with adjacent channels. This phenomenon is known as Inter-channel interference (ICI). To avoid ICI,

The remaining un-modulated subcarriers at both edges are used as guard bands between adjacent OFDM channels.

The $N_d + 1$ subcarriers in the center of the spectrum are modulated with data symbols $X_{i,n}$ before transmission. The remaining sub-carriers are guard bands and are usually left un-modulated. The OFDM modulation then can be expressed as in [1] by

$$x_k = \sum_{n=0}^{N-1} X_{i,n} e^{j2\pi nk/N}, \quad k = 0, 1, \dots, N-1 \quad (2.1)$$

where i is the OFDM symbol number and n is the sub-carrier number. (2.1) is recognized as the Inverse Discrete-time Fourier Transform (IDFT). Thus during modulation in the transmitter, IDFT can be used. Conversely during demodulation at the receiver, Discrete Fourier Transform (DFT) can be used. IFFT and FFT can serve as computationally faster alternatives to IDFT and DFT respectively.

A top-level description of a typical OFDM system is illustrated in Figure 2.2. After the IFFT in (2.1), the signal is oversampled at by factor OS and passed through a pulse shaping filter. The signal is then converted from discrete to continuous time for transmission through the wireless channel.

The signal $s(t)$ then goes through channel effects and the received signal can be given by

$$r(t) = s(t) \otimes h_C(t) + n(t) \quad (2.2)$$

where $h_C(t)$ is the channel impulse response, \otimes denotes linear convolution and $n(t)$ is Gaussian (assumed) noise in the channel.

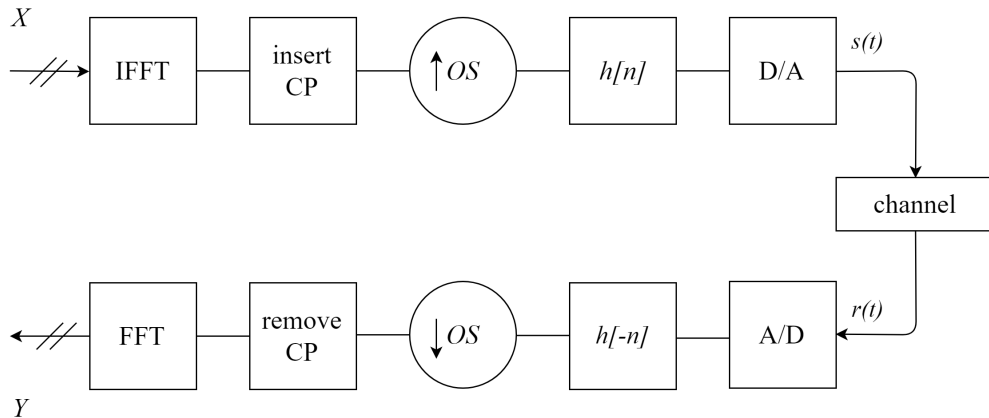


Figure 2.2: OFDM system block diagram

Cyclic prefix

Cyclic prefix (CP) is a key concept in OFDM which enables the simple channel estimation and equalization in the receiver. Typically, CP is a part of the time domain signal at the end that is copied to the front. Figure 2.3 illustrates the cyclic prefix in an OFDM symbol. CP can also be a sequence of zeros or un-modulated data points. The Length of the CP should be at least as long as the impulse response of the channel.

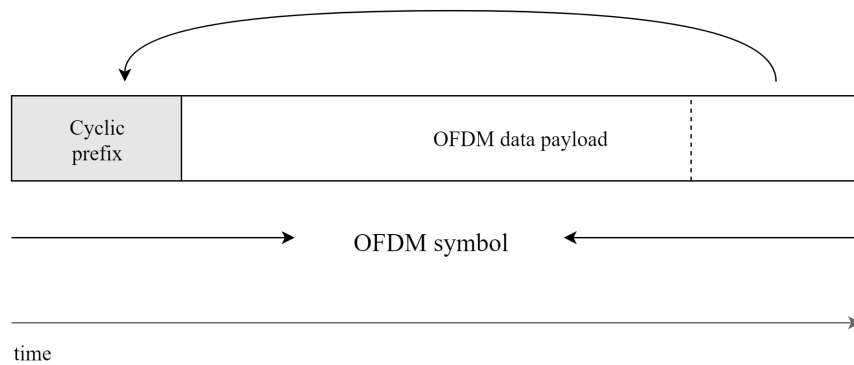


Figure 2.3: Cyclic prefix in an OFDM symbol

The CP serves two important purposes -

- If two consecutive OFDM symbols in a continuous stream of data in time domain overlap (Inter-symbol Interference), the CP prevents the data payload from being

compromised.

- In a slow fading frequency-selective channel (covered in chapter 3), copying part of the symbol to the front allows for the linear convolution in (2.2) to be modeled as circular convolution and subsequently converted into frequency domain using the DFT operation.

At the receiver, the signal goes through the reverse process of that in the transmitter. At the output of this FFT, the n^{th} subcarrier output for block i can be written as

$$Y_{i,n} = X_{i,n}H_{i,n} + N_{i,n}, \quad 1 \leq n \leq N_d \quad (2.3)$$

where $H_{i,n}$ is the frequency response of the channel obtained from $h_C(t)$. $N_{i,n}$ is channel noise, and will be independent, identically-distributed, and complex Gaussian. From (2.3), we can recover the transmitted signal by simply dividing Y by the channel frequency response. The level of noise however, will affect the accuracy of recovery.

2.2 OFDM channel modulation

The incoming serial stream of bits goes through a serial-to-parallel conversion while every bit is being converted into an M-ary QAM symbol. This parallel data is then mapped on to subcarriers to generate an OFDM frame after adding the guard intervals and pilot symbols at the appropriate subcarrier frequencies. This OFDM frame is then converted to a time domain signal using IFFT operation before inserting the cyclic prefix. The system then goes through the process explained in Figure 2.2.

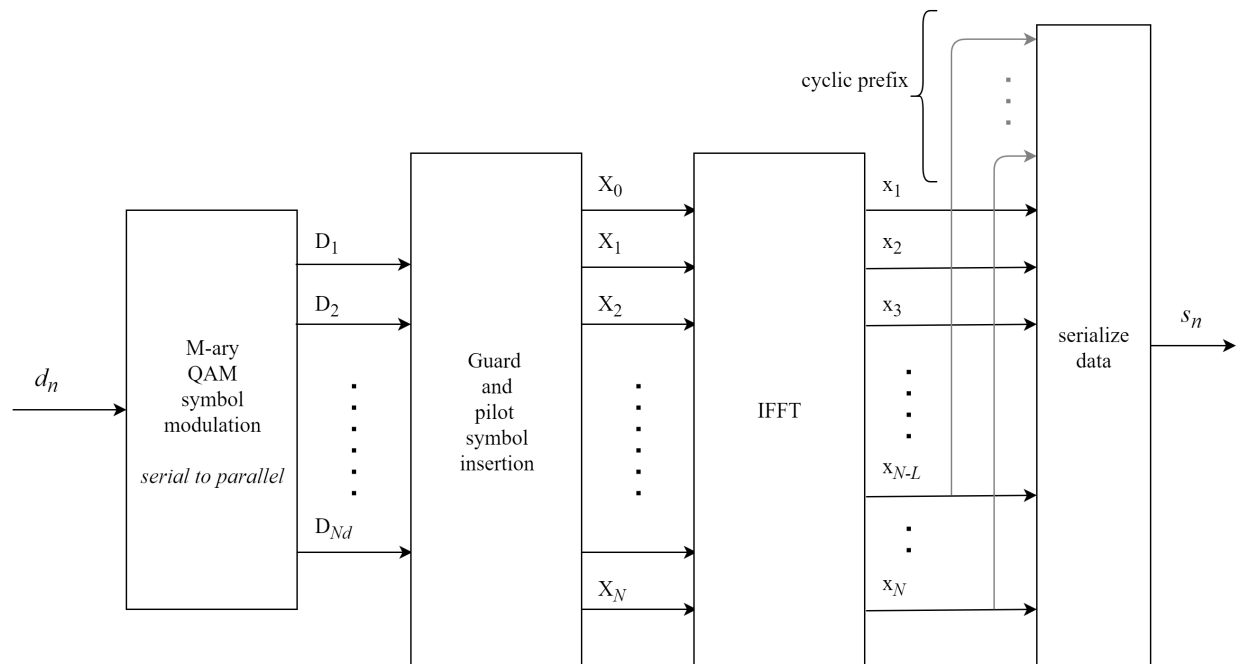


Figure 2.4: OFDM modulation block diagram

2.3 OFDM channel demodulation

The demodulation process at the receiver is similar to reversing the modulation procedure, except frame parsing (timing and frequency offset estimation) is required before demodulation and channel estimation is required after demodulation. The block diagram in Figure 2.5 describes this procedure.

The procedure of timing and frequency estimates is essential for frame parsing. The receiver uses these estimates to extract frames from the received data and then removes the cyclic prefix. Simulations in this thesis use the technique from [4] to obtain the timing and frequency estimates. This technique is not covered in this thesis. From here the data is handled in parallel fashion and the FFT operation is used to convert the data back into frequency domain. Pilot symbols are then extracted from this frequency domain data and used to estimate the channel frequency response. In this thesis we primarily concern

ourselves with using the pilot symbol information to estimate the rest of the frequency response of the channel. These estimates are used in compensation to recover transmitted data and then M-ary QAM decisions are performed to determine bit symbol errors in the system, if any.

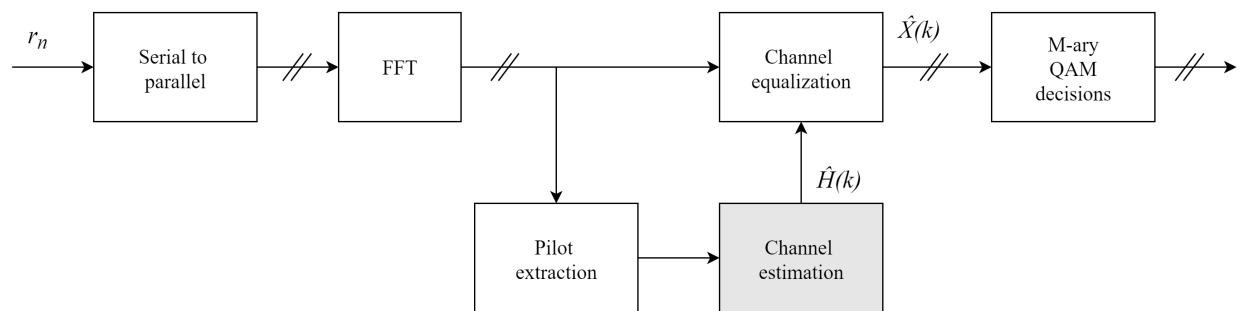


Figure 2.5: OFDM demodulation block diagram

Chapter 3

Wireless transmission channel

It is essential to assign an appropriate mathematical model to a channel in any communication system. This model will help understand the transformations a signal goes through in the channel and allow for exploring ways to improve the performance of the system.

In wireless communication channels, multiple paths of transmitted signals can be reflected off of surroundings. At the receiver antenna, the received signal is a combination of these multipath signals. The wireless channel affects the amplitude and phase of each of these signals differently and they add up to form a constructive and destructive pattern (multipath fading). Figure 3.1 shows a simple two-path plane earth reflection model in a wireless channel [1]. Here one path is direct and the other is received after reflecting from the earth's surface. This model can be expanded to have more paths reflecting from other surfaces in the surrounding (e.g. buildings, mountains, etc.). Adding to this degradation is the noise and possible frequency offsets present in the channel.

In this chapter, a general mathematical formulation of a physical channel is formed. Then the effects of multipath fading on a channel, especially on the frequency response are demonstrated. Other channel effects in a wireless channel are also discussed.

During propagation, a wireless signal goes through two types of fading effects:

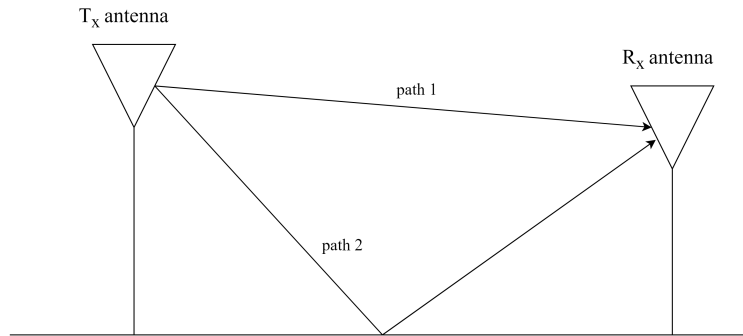


Figure 3.1: Two-path propagation model

- **Long-term (large-scale) fading:** Caused mainly due to reflections of multiple paths from the geographical surroundings (landscape, mountains, etc.). These types of fading effects vary slowly when compared to OFDM symbol time. They are characterized statistically by median path loss and lognormal shadowing. These effects are important in predicting the coverage and availability of a particular service.
- **Short-term (small-scale) fading:** Caused mainly due to the immediate environment (buildings, trees, etc.) and the movement of the mobile terminal. These effects last for a much shorter time than long-term fading effects. They are often characterized statistically by Rayleigh fading, under the assumption of many contributing scattering paths.

3.1 Channel model

A real-life wireless channel is time-dispersive and may also be time-varying in nature. A dispersive channel affects signals modulated at different frequencies differently and can also be referred as frequency selective. A general model for such a channel can be characterized by the complex baseband equivalent of the impulse response given by

$$\tilde{h}(t) = \sum_{l=1}^L \alpha_l(t) \delta(t - \tau_l(t)) \quad (3.1)$$

where L is the number of significant propagation paths, α_l is the complex gain for path l , τ_l is the corresponding time delay for the path at the receiver at time t and $\delta(t)$ is the Dirac function or the unit-impulse function. The complex gain values are relative to each other and reflect the distribution of power of each path at the receiver. The complex gains and time delays may vary with time or remain unchanged depending on the nature of the channel.

Wireless channels are broadly classified into four groups in [1] and [5] as

1. Non-selective (neither in frequency nor in time).
2. Frequency-selective (but not in time).
3. Time-selective (but not in frequency).
4. Time and frequency-selective.

Before we dive further into the different types of wireless channels, we introduce the concept of delay spread.

Delay spread

In a multipath channel, the multiple paths reflect from different surfaces and travel different amount of distances. These paths arrive at the receiver at different time and lead to spreading the received energy in time. Delay spread can be defined as the time spread between the arrival of the first and last significant multipath signal seen by the receiver. In case of the model in (3.1), the delay spread is $\tau_L - \tau_1$.

Delay spread can lead to inter-symbol interference (ISI) when the delayed multipath signals

overlap with symbols following in time. If the delay spread exceeds approximately 10% of the OFDM symbol duration, ISI experienced at the receiver reaches a significant level and causes reduction in achievable data rate [1].

3.1.1 Frequency-selective channels

In (3.1), consider the case where the complex gains and time delays do not vary with time. In practice, this is possible when the transmitter and receiver remain in their locations and there is no major change in the surroundings. The complex baseband equivalent of the impulse response for such a channel can be given by

$$\tilde{h}(t) = \sum_{l=1}^L \alpha_l \delta(t - \tau_l) \quad (3.2)$$

This channel is time-invariant but may be frequency selective. The frequency selective nature of the channel will be described using the channel frequency response in section 3.2. Figure 3.2 displays the impulse response model for a channel with three paths which may be frequency selective depending on the delay spread. It describes relative amplitude (or power) of the different paths and the time delay associated with them. The impulse response model for frequency-selective channels will remain unchanged.

3.1.2 Time-selective channels

As the name suggests, the characteristics of a time-selective channel change as a function of time. Thus α_l and τ_l are time-varying, and even the number of paths may change with time. Since α_l varies with time, received signal strength also varies with time. Impulse response model for such a channel is shown in Figure 3.3.

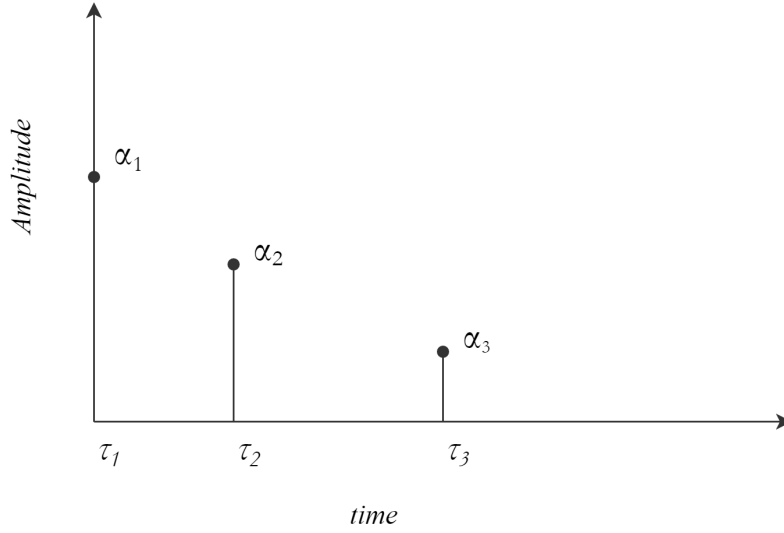


Figure 3.2: Impulse response model for a frequency-selective channel

3.2 Frequency response in multipath channels

In this section we discuss how multipath propagation affects the frequency response of a frequency-selective channel described in section 3.1.1. To get the baseband equivalent of the channel frequency response $\tilde{H}(f)$, we take the Fourier transform of the channel impulse response given in (3.2)

$$\tilde{H}(f) = \sum \alpha_l e^{-j2\pi f\tau_l} \quad (3.3)$$

In OFDM systems, the received signal in the frequency domain can be modeled as multiplication of the transmitted signal with the channel frequency response. Rewriting the frequency domain representation of the received signal from (2.3) in baseband equivalent form

$$\tilde{Y}_{i,n} = \tilde{X}_{i,n} \tilde{H}_{i,n} + N_{i,n}, \quad 1 \leq n \leq N_d$$

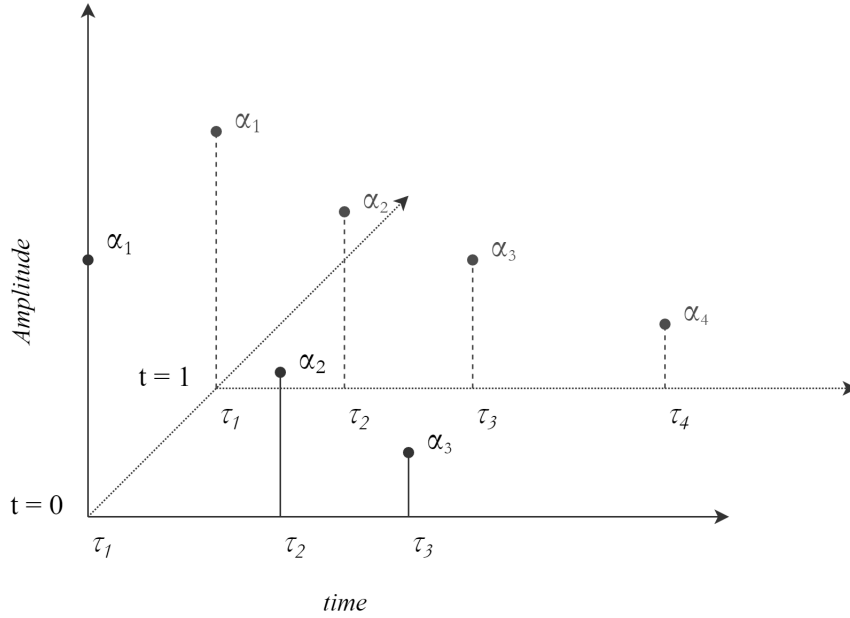


Figure 3.3: Impulse response model for a time-selective channel

where $H_{i,n}$ is the baseband channel frequency response and $N_{i,n}$ is the additive white Gaussian noise at the i^{th} OFDM symbol and n^{th} sub-carrier. An ideal wireless channel would be one which does not distort the signal passing through it. For this response to be ideal, it would have to have unit magnitude and linear phase. Figure 3.4 shows the magnitude and phase response of an ideal channel in the frequency domain in the absence of noise. This channel is considered as a flat channel. Notice there are N_g guard symbols at both edges of the band which are not modulated with data.

The physical impulse response corresponding to this channel is

$$\tilde{h}(t) = \delta(t)$$

There is no multipath phenomenon in this channel and the transmitted signal can be perfectly recovered as noise in the system is assumed to be absent. Real-life channels, as expected, are far from ideal and are subjected to multipath fading, frequency offsets and noise. We now explore the effect of multipath fading on channel frequency response.

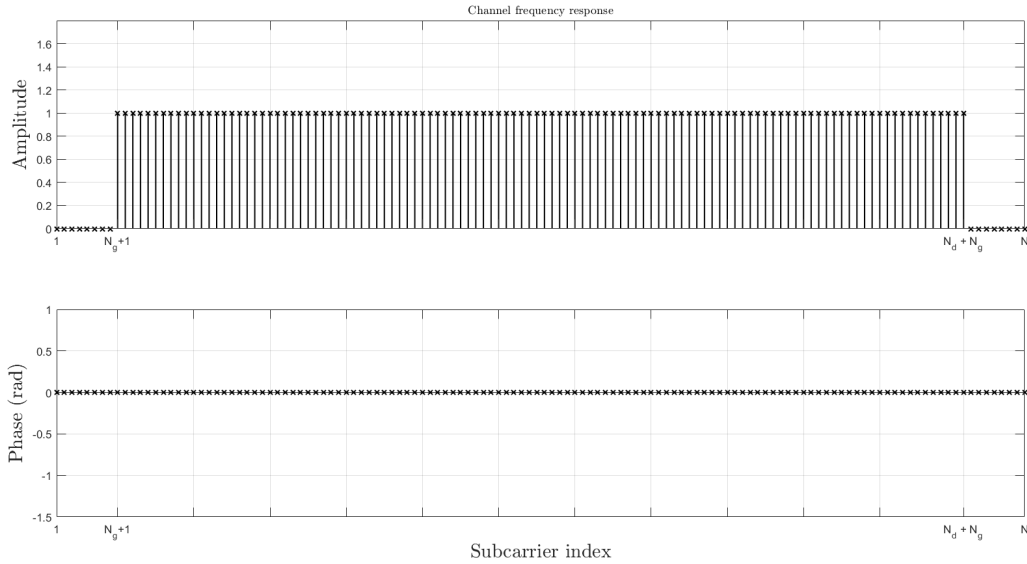


Figure 3.4: Ideal channel frequency response

As mentioned before, multipath propagation of signals in wireless channels can cause the channel frequency response to be frequency-selective. Figure 3.5 shows the channel frequency response for a two-path channel

$$\tilde{h}(t) = 0.9\delta(t) + 0.5e^{-j\pi/5}\delta(t - 2\mu s)$$

As can be seen, there are phase distortions in addition to magnitude distortions caused by the interference pattern of the signal at the receiver. The fact that the channel response is not flat means that the received signal will differ from the transmitted signal by more than just a scaling factor and noise.

Consider a more severe multipath case of a 4-path model illustrated in Figure 3.6

$$\tilde{h}(t) = 0.8\delta(t) + 0.5e^{-j\pi/5}\delta(t - 2\mu s) + 0.3e^{j\pi/4}\delta(t - 4\mu s) + 0.2e^{j\pi/8}\delta(t - 6\mu s)$$

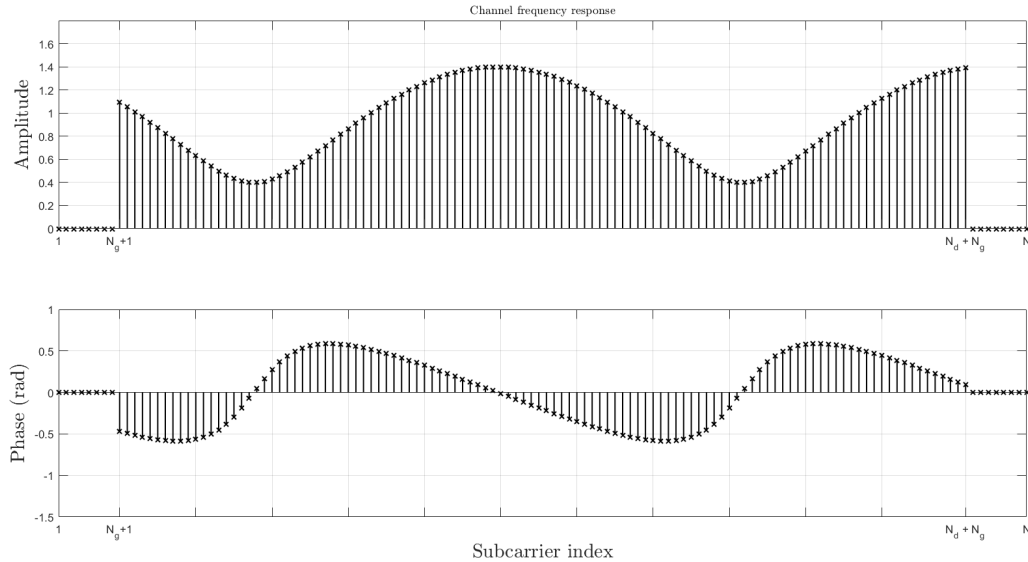


Figure 3.5: Two-path channel frequency response

From Figures 3.5 and 3.6 we can see the frequency selective nature of the channel frequency response caused by multipath propagation.

In the frequency domain, the channel frequency response $H_{i,n}$ is directly multiplied with the transmitted signal $X_{i,n}$. Thus the received signal will have all the amplitude variations and phase fluctuations in addition to the noise present in the system. Note we are not considering any frequency offsets here.

At the receiver, we attempt to recover the transmitted signal by dividing $Y_{i,n}$ by $H_{i,n}$. In wireless channels, the frequency response is not only frequency selective, but may also be time varying. This means the number of paths (and thus the frequency response) may change from time-to-time. This makes it impossible for the receiver to know the CFR before hand. This is why channel estimation is an important problem. Channel estimation techniques will be covered in detail in the next chapter.

The time delays and phase associated with different paths in the 2-path and 4-path models

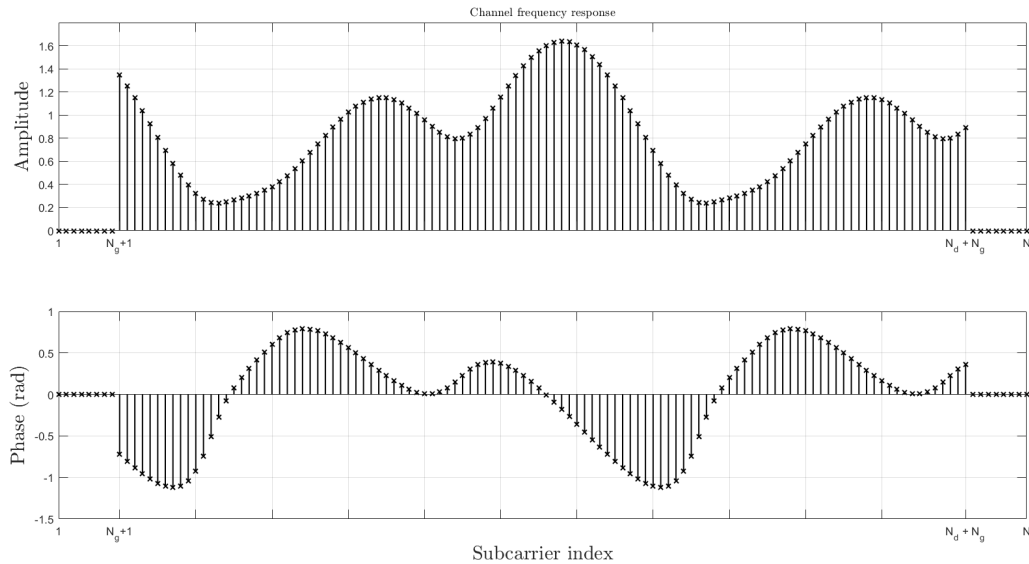


Figure 3.6: Four-path channel frequency response

are chosen arbitrarily. Changing these values would produce different plots but tell the same story.

3.3 Other propagation characteristics

In this section, we look at other phenomena that affect a signal in the transmission channel. They are important considerations in all the simulations performed for this project, but are not the focal point of research in this thesis.

3.3.1 Noise

In a general sense, noise is the unwanted electrical interference that a signal endures in a wireless channel. Noise can occur due to two types of sources given below.

- **Natural sources** such as atmospheric disturbance, extra-terrestrial background radiation, thermal noise, electronic noise, etc.
- **Artificial sources** such as switching transients, multi-access interference, etc.

In our mathematical model, we consider all noise to be accumulated into one variable (the N vector in equation (2.3)) and this vector is assumed to be complex normally distributed with independent components.

3.3.2 Frequency offset

There are two possible causes of frequency offsets at the receiver [4], [6]:

1. Mismatch between the oscillators at the transmitter and receiver.
2. Doppler shift.

Doppler effect arises due to the movement of either the transmitter or receiver. Suppose a receiver is moving away from the stationary transmitter. The received signal appears at a frequency lower than the actual carrier frequency. Opposite change occurs if the receiver is moving towards the transmitter. This change in the frequency is known as Doppler effect.

Doppler shift f_D can be given by

$$f_D = -f_C \frac{v}{c} \cos\theta \quad (3.4)$$

where f_C is the actual carrier frequency, v is the velocity of the receiver, c is the velocity of light and θ is the angle between velocity of the receiver and the straight line joining the receiver with the transmitter.

Frequency offsets are considered in simulations presented in this thesis and scheme used by authors in [4] is used to compensate for them.

Inter-channel interference

Frequency offsets may lead subcarriers at the edge of an OFDM symbol to interfere with the subcarriers in adjacent OFDM symbol (in frequency domain). This phenomenon is defined as inter-channel interference (ICI). Guard bands (un-modulated subcarriers) are used to tackle ICI.

Chapter 4

Channel estimation

Channel estimation is the process of learning the effect of the physical channel (described in chapter 3) on the transmitted data. It allows the receiver to account for the various channel effects the signal might go through, such as multipath fading, frequency offsets, noise interference, etc. In OFDM systems, equalization at the receiver is simplified as a frequency-selective channel is converted into a collection of flat-fading sub-channels. But the complex channel gain at each sub-carrier frequency is required for equalization. As estimating the channel (to a certain degree of error) allows for this equalization, channel estimation is essential in receiver design. In this chapter, we focus on estimating the channel frequency response which is affected by noise and multipath fading. To compensate for frequency offsets, we adopt the work done in [4].

Channel estimation techniques are reviewed extensively in [2] and [7] and can be broadly classified into four main categories:

1. *Channel frequency response* (CFR)-based estimation.
2. *Parametric model* (PM)-based estimation.
3. *Iterative channel estimation* (ICE).
4. Channel estimation in multiple-input multiple-output MIMO-OFDM systems.

CFR-based techniques have been the traditional approach to channel estimation in OFDM systems and have also been adopted widely into other commercial systems due to their simplicity [2]. In these techniques, the CFR at the pilot symbol frequencies is estimated first and then the CFR for the data symbols is estimated using decision-based tracking or interpolation algorithms.

For PM-based techniques, such as in [8], the channel is first modeled using a set of parameters. The channel estimation procedure involves estimating these parameters and then reconstructing the channel response. These techniques are more suitable when the channel being considered has a few dominant paths (say two to six). PM-based techniques, along with ICE can provide better performance in estimation and are considered to be advanced channel estimation techniques.

MIMO-OFDM systems are out of scope of research for this thesis and will not be discussed. ICE techniques, which use error-control coding to improve the channel estimates in an iterative manner, are also not discussed.

In cases where the channel is slow-fading in nature, differential encoding and detection on each subcarrier is possible and can serve as an alternative to channel estimation [1]. This has been explored in [9], and though the implementation is relatively easier a significant loss (3-4 dB) in signal-to-noise ratio (SNR) will result.

In this chapter, the channel estimation techniques used in this thesis are described in detail. Other existing techniques are also briefly covered.

4.1 CFR-based estimation

To help estimate the channel frequency response in OFDM systems, certain sub-carriers are modulated with a known amplitude (generally higher than the highest amplitude in the M-ary QAM modulation being used). These symbols are known as pilot symbols, and their corresponding sub-carrier frequencies are known as pilot frequencies. At the receiver, we can get an idea about the pattern of distortions across the entire OFDM symbol bandwidth by observing the pattern of the pilot symbols. We can then obtain the entire channel response by filling in the values between the pilot symbols. Figure 4.1 shows two popular schemes for loading pilot symbols. Scheme in Figure 4.1a is a ‘block’-type scheme where pilot symbols are loaded into all the sub-carriers in periodic time intervals. In this scheme, the estimated CFR is very close to the actual CFR at that time instant, but if the channel is time-varying in nature the estimated CFR loses accuracy and the equalization suffers. The scheme in Figure 4.1b describes a ‘comb’-type pilot arrangement in which pilot symbols are assigned in every OFDM symbol (in the frequency domain). In this case, even if the channel is time-varying we can get a reliable estimate of the CFR for a given symbol. More pilots in an OFDM symbol would help derive a more accurate CFR estimate at the cost of data throughput. A hybrid of these schemes can also be used (e.g. LTE).

Many techniques exist to estimate the channel frequency response using pilot symbols [2] [10], the easiest to implement being interpolation. The signals we deal with are complex in nature and we do interpolation in the complex plane. Before discussing the two types of interpolation techniques explored, we describe pilot symbols and their distribution across the OFDM block.

We assume a ‘comb’-type pilot arrangement with M pilots distributed equally across the

the i^{th} OFDM symbol.

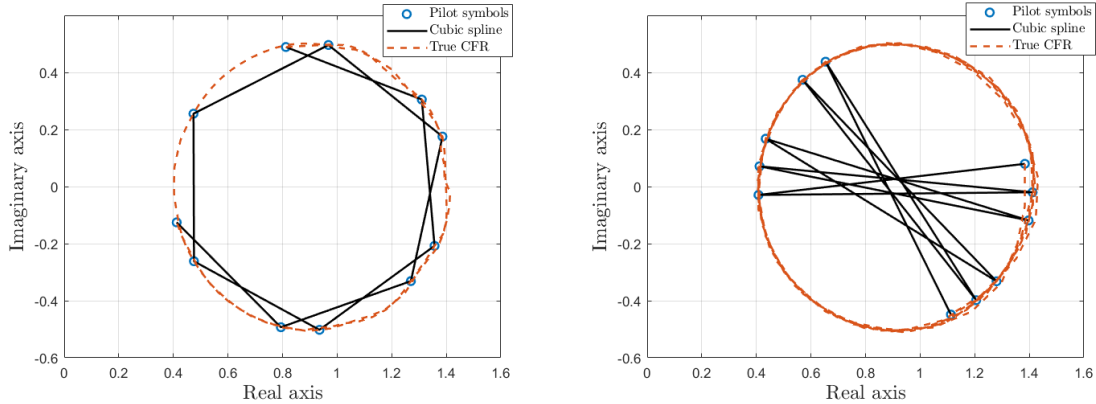
4.1.1 Linear interpolation

Linear interpolation is the simplest method to estimate CFR from pilot symbols. This is done by finding the slope between the raw channel estimates at the two nearest pilot sub-carriers in the complex plane and joining them by a straight line. Figure 4.2 shows CFR estimates using linear interpolation and the true CFR for a 2-path model (assuming no noise) with complex equivalent channel impulse response whole delay spread is $2\mu s$ (with pilot spacing in frequency domain of 7.8 kHz in our simulations).

$$\tilde{h}(t) = 0.9\delta(t) + 0.5e^{-j\pi/5}\delta(t - 2\mu s) \quad (4.4)$$

The “true” frequency response can be found by taking the Fourier transform (FFT or DFT) of $\tilde{h}(t)$ which is smoothly changing in amplitude and phase, as can be seen from the dotted line in Figure 4.2. We can see that linear interpolation provides a poor fit at a relatively low delay spread of $2\mu s$ and gets worse when the delay spread increases to $6\mu s$. Note that the interpolation fits perfectly through the pilot symbols. It will also fit the pilots in the presence of noise, which will worsen the already poor fit.

Although linear interpolation never provides a perfect estimate in non-ideal channels, it is the simplicity of the solution that is attractive. Some additional gain may be obtained by averaging the noisy pilot measurements using a sliding window over OFDM symbols. But the estimate using linear interpolation is already poor in a noise-less system and we can expect worse estimation if the true response varies significantly between pilots, i.e., with larger delay spread.



(a) Delay spread = 2 μs , $E_b/N_0 = 60$ dB (b) Delay spread = 6 μs , $E_b/N_0 = 60$ dB

Figure 4.2: Linear interpolation between pilots of a 2-path channel in (4.4)

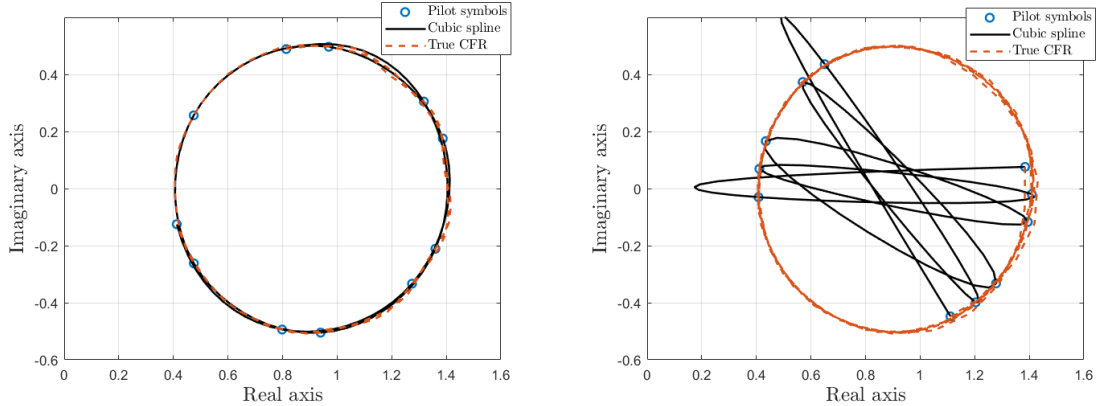
4.1.2 Cubic spline interpolation

Cubic splining [11] attempts to fit a smoother curve through the pilots, and a cubic spline will produce estimates that have continuous first and second derivatives, using piecewise third-order polynomials which pass through the M pilot symbols. The equation for representing the i^{th} segment [11] of the spline is

$$S_i(n) = a_i + b_i n + c_i n^2 + d_i n^3, \quad n \in [0, D_p] \quad (4.5)$$

where the set of coefficients is unique for every interval between two consecutive pilots. The second derivative of each polynomial (S_i) is set to zero at the endpoints and provides a boundary condition that completes the system of $M - 2$ equations. This leads to a tridiagonal system which is then solved to get the coefficients of the spline segments, followed by evaluating these splines at desired intermediate points, [11], [12].

Being a smoother interpolating process, cubic splining should produce better channel frequency response estimates, and it does so at high SNR, as shown in Figure 4.3. Cubic spline provides a good fit for a delay spread of 2 μs (metrics in Chapter 5) but when the



(a) Delay spread = $2 \mu s$, $E_b/N_0 = 60$ dB (b) Delay spread = $6 \mu s$, $E_b/N_0 = 60$ dB

Figure 4.3: Cubic spline interpolation between pilots of a 2-path channel in (4.4)

delay spread increases to $6 \mu s$ it cannot track the CFR correctly anymore.

4.2 PM-based estimation

Another way of estimating the channel frequency response relies on the model-based ESPRIT algorithm. In this section we replay the development in [8]. The first step identifies the multipath time delays $\{\tau_l\}$ in

$$h(t) = \sum_{l=1}^L \alpha_l \delta(t - \tau_l)$$

Once these are found, linear estimation methods produce the impulse response coefficients, and then the discrete Fourier transform gives the desired $H_{i,n}$.

Pilot subcarriers defined in (4.3) are again used to obtain channel frequency response at

the pilot subcarrier frequencies as

$$\begin{aligned} H'_{i,p(m)} &= \frac{Y_{i,p(m)}}{\Lambda_m} = H_{i,p(m)} + N_{i,p(m)}/\Lambda_m \\ &= \sum_{l=1}^L h_l(iT_s) e^{-j2\pi \frac{p(m)\tau_l}{NT}} + N_{i,p(m)}/\Lambda_m \end{aligned} \quad (4.6)$$

where $H'_{i,p(m)}$ is modeled as the summation of the complex-valued sinusoidal signals plus the complex white noise. Let $\mathbf{H}'_{i,P} = [H'_{i,p(0)}, \dots, H'_{i,p(M-1)}]^T$ where $(\cdot)^T$ represents transpose operation. Values in this vector are then arranged in the following way to form a snapshot array:¹

$$\mathbf{Q}_i = \begin{bmatrix} H'_{i,p(0)} & H'_{i,p(1)} & \cdots & H'_{i,p(K-1)} \\ H'_{i,p(1)} & H'_{i,p(2)} & \cdots & H'_{i,p(K)} \\ \vdots & \vdots & \cdots & \vdots \\ H'_{i,p(M-K)} & H'_{i,p(M-K+1)} & \cdots & H'_{i,p(M-1)} \end{bmatrix} \quad (4.7)$$

Then a sample correlation matrix is obtained from the forward-backward approach [13] as

$$\mathbf{R}_i = \frac{1}{2K} (\mathbf{Q}_i \mathbf{Q}_i^H + \mathbf{J} \mathbf{Q}_i \mathbf{Q}_i^H \mathbf{J}) \quad (4.8)$$

where (\cdot) denotes complex conjugate, $(\cdot)^H$ denotes Hermitian transpose and \mathbf{J} is a matrix with 1's on the anti-diagonal and 0's elsewhere. Eigenvalue decomposition of \mathbf{R}_i yields

$$\mathbf{R}_i = \sum_{k=1}^{k=M-K+1} \lambda_k \mathbf{u}_k \mathbf{u}_k^H \quad (4.9)$$

where $\lambda_1 \geq \dots \geq \lambda_{M-K+1}$ are the eigenvalues and $\mathbf{u}_1, \dots, \mathbf{u}_{M-K+1}$ are the corresponding eigenvectors. We note that the number of rows in \mathbf{Q} , and thus the size of the square matrix \mathbf{R} , must satisfy $M - K \geq L$ for identifiability.

The maximum number of significant paths in the channel, L , is assumed to be known (in

¹Averaging of pilots over OFDM symbols could be done to reduce effect of noise.

our testing, we set $L = 3$). First, the ESPRIT method is used to acquire the time delays. The eigenvectors corresponding to the L largest eigenvalues of \mathbf{R}_i are organized into a matrix $\mathbf{U} = [\mathbf{u}_1, \dots, \mathbf{u}_L]$. Then matrices \mathbf{U}_1 and \mathbf{U}_2 are formed as

$$\mathbf{U}_1 = [\mathbf{I}_{M-K}, \mathbf{0}]\mathbf{U} \quad (4.10)$$

and

$$\mathbf{U}_2 = [0, \mathbf{I}_{M-K}]\mathbf{U} \quad (4.11)$$

where \mathbf{I}_{M-K} is an identity matrix of dimension $(M - K) \times (M - K)$ and \mathbf{U}_1 and \mathbf{U}_2 have dimensions $(M - K) \times L$. We now form the matrix ϕ as

$$\phi = (\mathbf{U}_1^H \mathbf{U}_1)^{-1} \mathbf{U}_1^H \mathbf{U}_2 \quad (4.12)$$

After we find the L eigenvalues $\{\nu_l\}_{l=1}^L$ of the matrix ϕ , the l th path time delay is given by

$$\hat{\tau}_l = \frac{N}{(2\pi D_p)T} \arg(\nu_l^*), \quad l = 1, \dots, L \quad (4.13)$$

where $\arg(\nu_l^*)$ denotes the phase angle of ν_l^* in the interval $[0, 2\pi)$ and ν_l^* denotes the complex conjugate of ν_l .

Using the estimated time delays, (4.6) can be rewritten as

$$\mathbf{H}'_P = \mathbf{W}_P \mathbf{h} + \mathbf{N}_P \quad (4.14)$$

where

$$\mathbf{W}_P = \begin{bmatrix} e^{-j2\pi \frac{p(0)\hat{\tau}_1}{NT}} & \dots & e^{-j2\pi \frac{p(0)\hat{\tau}_L}{NT}} \\ \vdots & \ddots & \vdots \\ e^{-j2\pi \frac{p(M-1)\hat{\tau}_1}{NT}} & \dots & e^{-j2\pi \frac{p(M-1)\hat{\tau}_L}{NT}} \end{bmatrix} \quad (4.15)$$

is the Fourier transform matrix, \mathbf{h} is the vector of multipath gains to be estimated and \mathbf{N}_p

is the noise vector. [8] describes use of MMSE estimation of \mathbf{h} , but lacking a model for the covariance of channel coefficients, we use a least-squares estimator based on (17):

$$\mathbf{h} = \left(\mathbf{W}_P^H \mathbf{W}_P \right)^{-1} \mathbf{W}_P \mathbf{H}'_P \quad (4.16)$$

The estimator for the entire channel frequency response is then given by

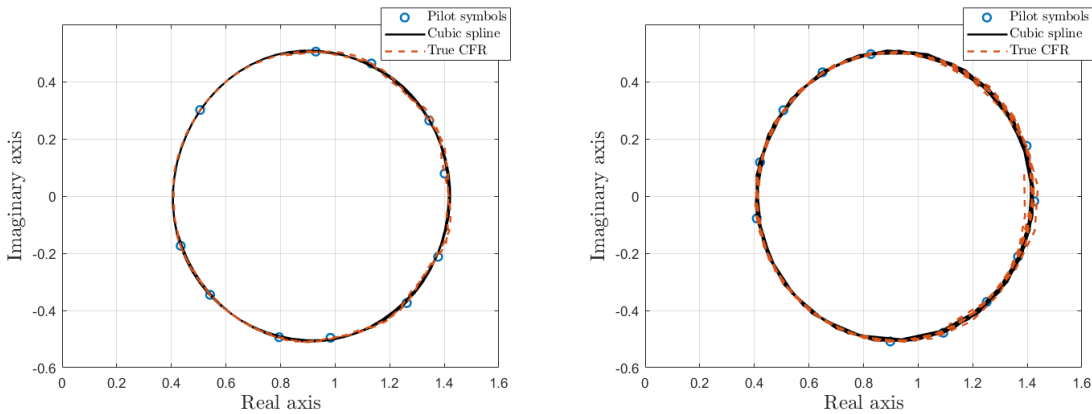
$$\hat{\mathbf{H}} = \mathbf{W}_H \mathbf{h} \quad (4.17)$$

where

$$\mathbf{W}_H = \begin{bmatrix} e^{-j2\pi \frac{-Nu/2}{N} \frac{\hat{\tau}_1}{T}} & \dots & e^{-j2\pi \frac{-Nu/2}{N} \frac{\hat{\tau}_L}{T}} \\ \vdots & \ddots & \vdots \\ e^{-j2\pi \frac{-Nu/2}{N} \frac{\hat{\tau}_1}{T}} & \dots & e^{-j2\pi \frac{-Nu/2}{N} \frac{\hat{\tau}_L}{T}} \end{bmatrix} \quad (4.18)$$

is the Fourier transform matrix and $\hat{\mathbf{H}}$ is the estimated channel frequency response.

Figures 4.4a and 4.4b show the CFR estimates from the ESPRIT-based technique for $2\mu s$ and $6\mu s$ delay spreads respectively. We can see that this estimation technique closely follows the true response even at high delay spread. ESPRIT method does have an upper threshold in terms of handling delay spreads which will be discussed in chapter 5.



(a) Delay spread = $2 \mu s$, $E_b/N_0 = 60$ dB (b) Delay spread = $6 \mu s$, $E_b/N_0 = 60$ dB

Figure 4.4: ESPRIT estimation for pilots of a 2-path channel in (4.4)

Clearly the computational complexity for this method is larger than both the interpolation methods and involves several distinct linear algebraic procedures. Number of paths L and the variable K are the “drivers” of complexity in this method. K decides the number of computations in (4.7)-(4.12) and L decides the number of computations in (4.10)-(4.17). More discussion about the complexity and accuracy of these algorithms will be discussed later in this thesis.

Chapter 5

Simulation and results

In this chapter, we compare the performance of the three channel estimation techniques explored in this thesis. This comparison is based on three factors

1. Closeness of the estimated CFR with the ‘true’ CFR. In simulations, the true CFR can easily be calculated by taking the FFT of the channel impulse response being used. We use a RMSE metric to quantify this closeness.
2. Time required for each technique to estimate the CFR.
3. Symbol error rate (SER) of the system with the CFR estimate being used compared to the ideal SER performance of the system.

Before looking at the results, we first define some of the important system parameters being used in the simulations in table 5.1

5.1 Results

All the simulation results displayed in this chapter are implemented in Mathworks MATLAB[®] and when available, MATLAB functions are utilized. We use multiple protocol OFDM

Application System Parameters	
Total Bandwidth:	320 MHz
Number of Channels:	256
Channel Spacing:	1.25 MHz
Root-Nyquist Roll-off Factor:	0.25
Modulation Type:	OFDM
Constellation:	M-ary QAM (square)
FFT Size:	128
Cyclic Prefix Overhead:	12.5% (16 Symbols)
Subcarrier Spacing:	7.8 kHz
Data Subcarriers:	100
Guard Subcarriers:	16 + null DC subcarrier
Pilot Tones:	11

Table 5.1: System Parameters

frames in an end-to-end simulation of a wireless communication system, with careful calibration for additive white Gaussian noise.

5.1.1 Effect of delay spread on the channel and estimation

Consider the base-band complex envelope of a channel

$$\tilde{h}(t) = 0.9\delta(t) + 0.5e^{-j\pi/5}\delta(t - D\mu s) \quad (5.1)$$

where D is a variable time delay for the second path. Delay spread for this channel is always $D \mu s$.

Effect of changing the delay spread in the channel on the estimation techniques is demonstrated in Figure 5.1. These figures represent magnitudes of the frequency responses (estimated and true) at high SNR ($E_b/N_0 = 60$ dB). These responses are for the two-path model for three different time delays (2,4 or 6 μs) for the second path. For delay spread

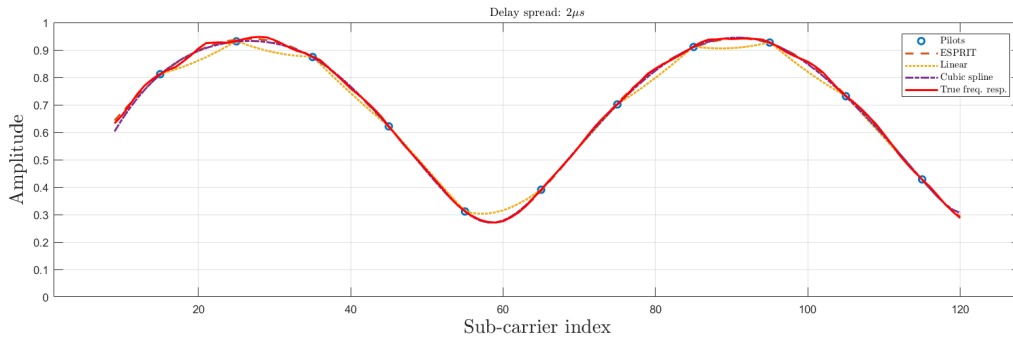
of $2 \mu s$, all estimates for the frequency response are fairly similar and follow the true response within an acceptable error. But at larger delay spread, the true frequency response changes more rapidly which the interpolation techniques cannot correctly reproduce and thus do not provide a good fit for the estimated response (This is an under-sampling effect across the frequency domain.). This error, compounded with the already existing penalty for multipath fading, degrades the symbol performance for the interpolation techniques which will be demonstrated. The ESPRIT-based method, however, tracks the response satisfactorily in all three cases.

As the delay spread increases, the performance of all three techniques worsens. After a certain amount of delay spread, we start observing errors in the system even when no noise is present. Figure 5.2 shows the probability of symbol error (P_s) against the increasing delay spread. Here linear interpolation is used to estimate the channel, but the same story follows for other estimation techniques.

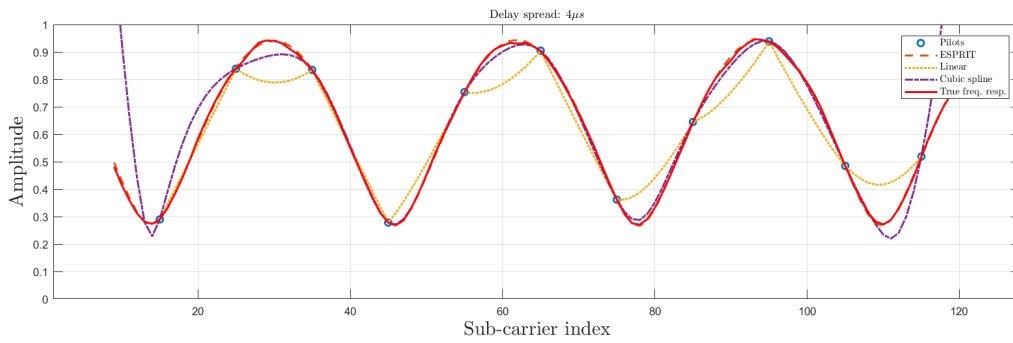
For all three estimation techniques, same set of pilots are used. To improve the linear and cubic spline interpolation estimates, pilots may be placed at both edges of the data carriers to avoid the estimate overshoots visible in Figures 5.1b and 5.1c.

5.1.2 M-ary QAM constellations

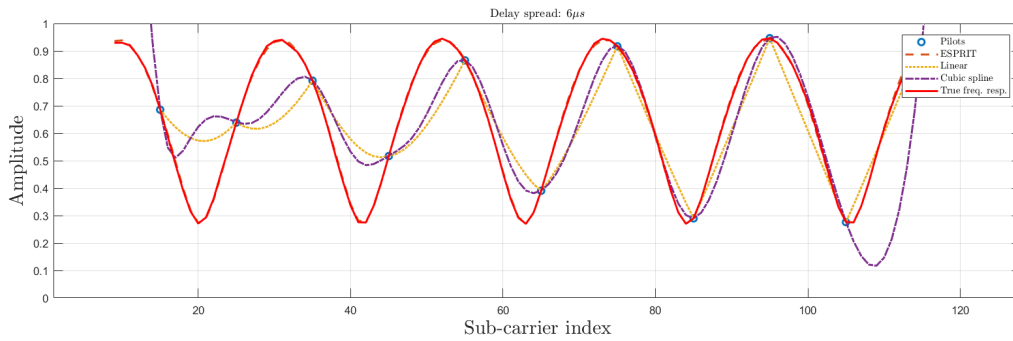
Next we compare the equalized constellations for different delay spreads for all three estimation techniques. Figure 5.3 shows constellations for a 16-QAM scheme for high and low SNR for the model in equation (5.1). Figure 5.4 shows the same for a 4-QAM (QPSK) scheme. For a delay spread of $2 \mu s$, all three estimation techniques produce decent constellations, among which the one from the ESPRIT-based algorithm is the best. As the delay spread increases, the constellations produced from the interpolation techniques become more disorganized. This is due to the poor estimates produced by interpolation



(a) Delay spread = $2 \mu s$, $E_b/N_0 = 60$ dB



(b) Delay spread = $4 \mu s$, $E_b/N_0 = 60$ dB



(c) Delay spread = $6 \mu s$, $E_b/N_0 = 60$ dB

Figure 5.1: (a) Effect of changing delay spread on the true CFR and estimated CFRs

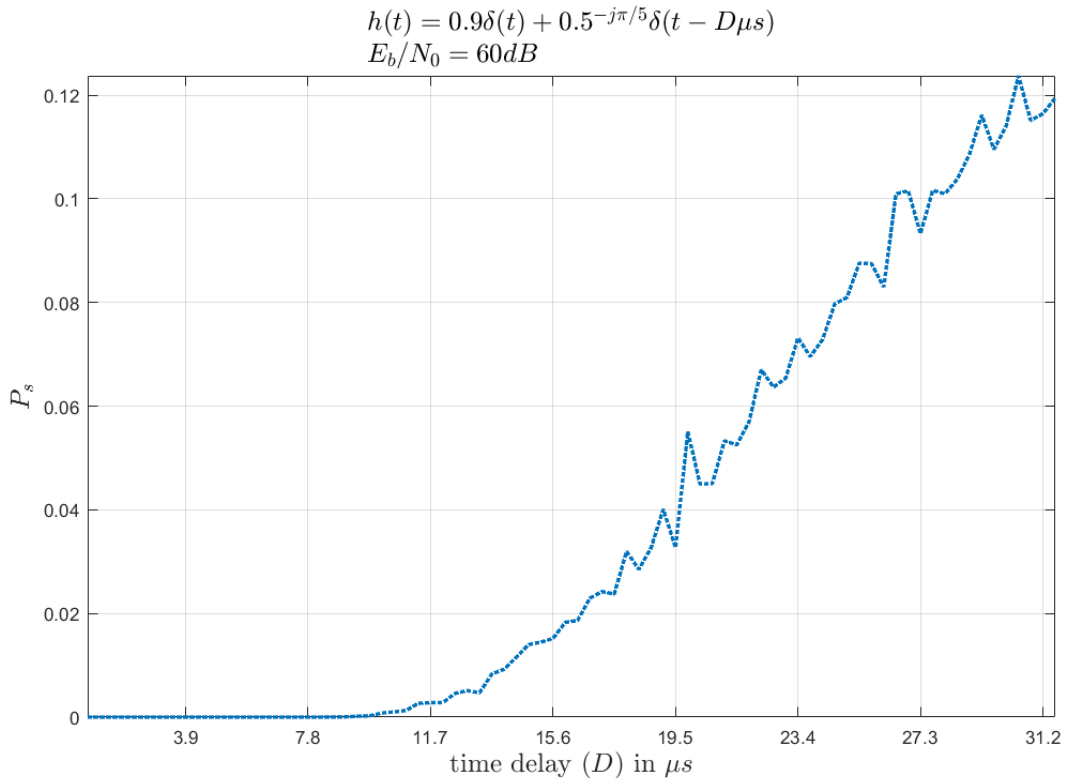
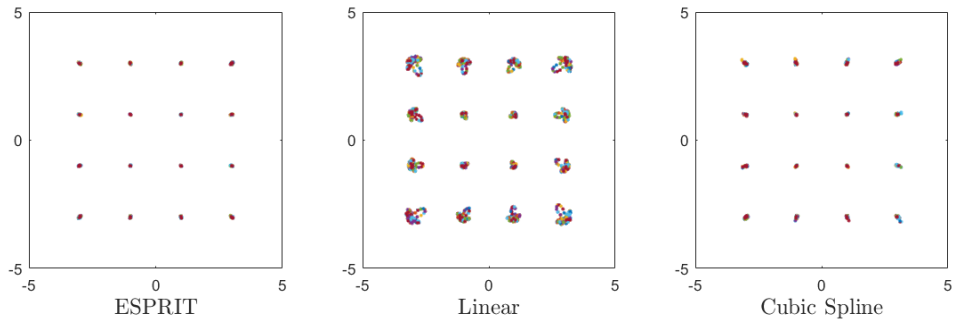


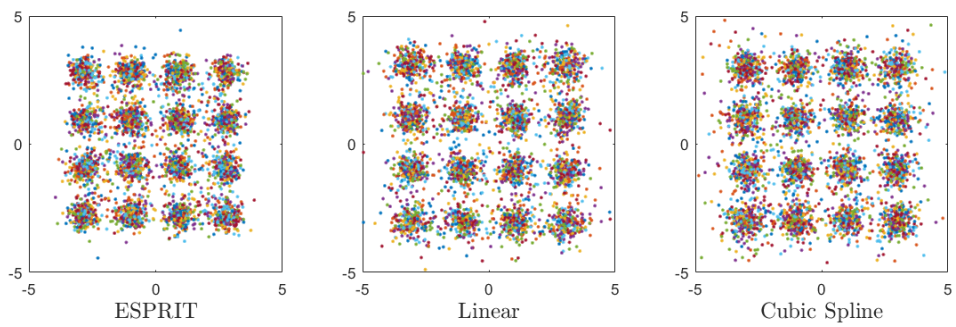
Figure 5.2: Effect of increasing the delay spread on the probability of error ($E_b/N_0 = 60$ dB, linear interpolation)

techniques which are then used in the equalization process. Thus Figures 5.3 and 5.4 concur with the frequency response plots in Figure 5.1. At high SNR values, these constellations may be considered acceptable, at least for QPSK, even though not perfect. But increasing noise in the channel causes scattering of the constellation points and they are likely to cross decision boundaries and cause errors at the receiver which can be demonstrated by Figures 5.3b and 5.3d. A similar pattern follows when QPSK modulation scheme is used, as can be seen in Figures 5.4b and 5.4d.

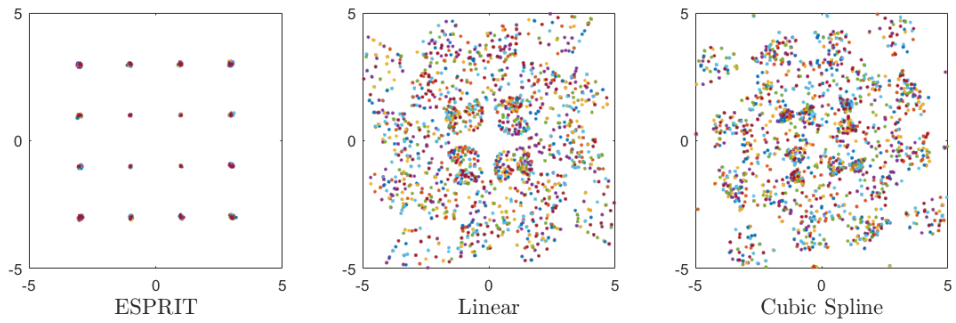
To quantify the differences between the CFR estimates and the “true” frequency responses we calculate the time required for each method to estimate the CFR. The time was calculated on a computer using the following processor: *intel(R) core(TM) i7-6500U CPU @ 2.5GHz*. We also define a root mean square error (RMSE) metric. Suppose the true CFR is H_{true}



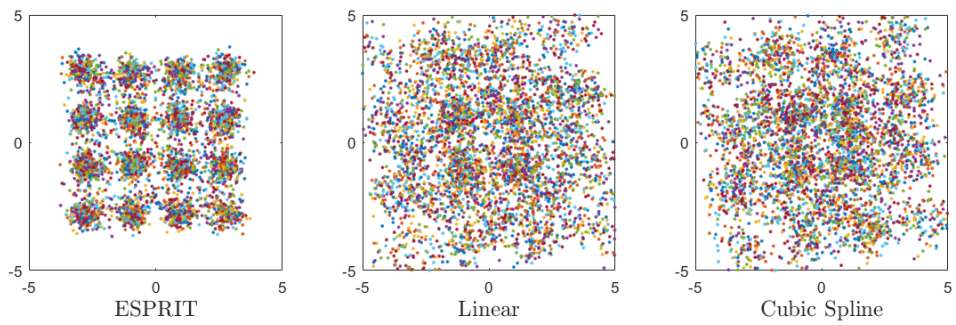
(a) Delay spread = $2\mu s$, $E_b/N_0 = 60$ dB



(b) Delay spread = $2\mu s$, $E_b/N_0 = 15$ dB

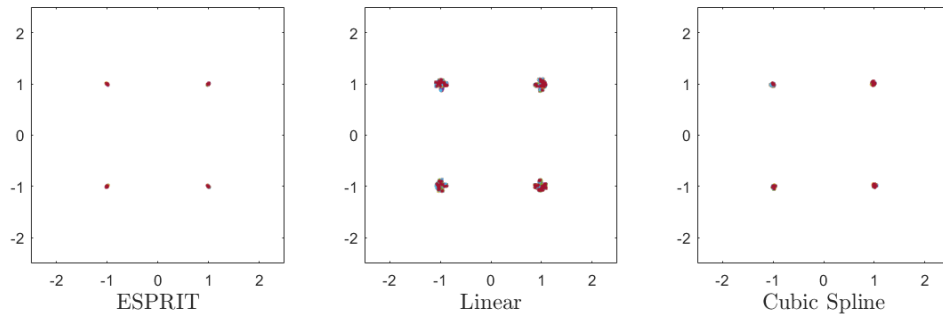


(c) Delay spread = $6\mu s$, $E_b/N_0 = 60$ dB

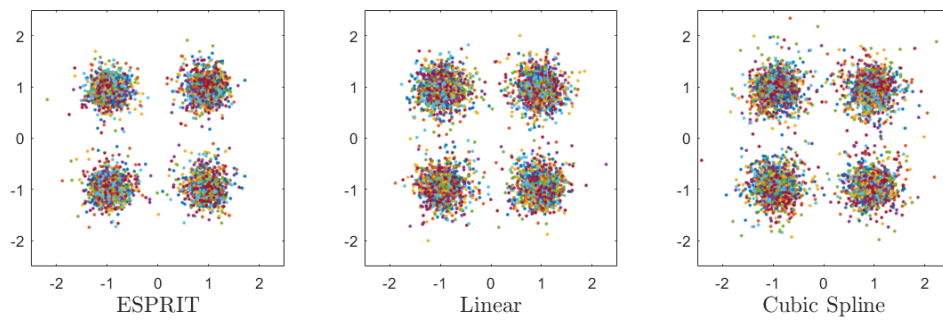


(d) Delay spread = $6\mu s$, $E_b/N_0 = 15$ dB

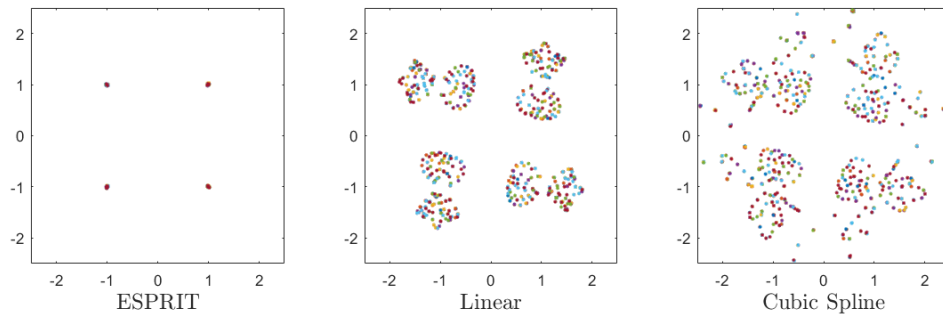
Figure 5.3: Constellations for 16-QAM. Left to right: ESPRIT, Linear, Cubic Spline.



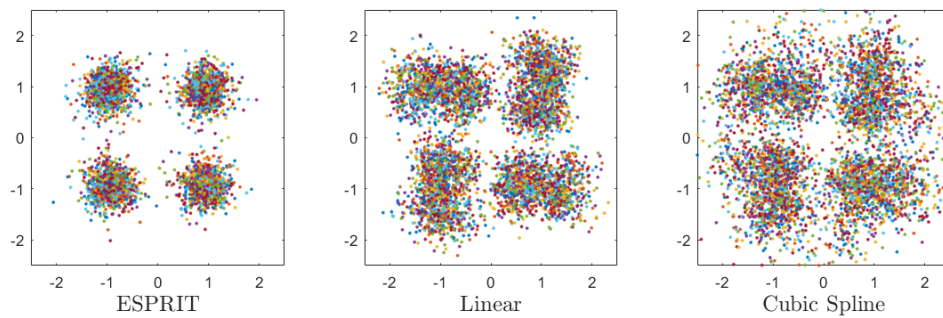
(a) Delay spread = $2\mu s$, $E_b/N_0 = 60$ dB



(b) Delay spread = $2\mu s$, $E_b/N_0 = 15$ dB



(c) Delay spread = $6\mu s$, $E_b/N_0 = 60$ dB



(d) Delay spread = $6\mu s$, $E_b/N_0 = 15$ dB

Figure 5.4: Constellations for 4-QAM (QPSK modulation). Left to right: ESPRIT, Linear, Cubic Spline.

and the estimated CFR is H_{est} . Then the normalized RMSE is given by

$$RMSE = \sqrt{\frac{\sum_{j=1}^{N_d} \sum_{i=1}^n |H_{\text{true}} - H_{\text{est}}|^2}{\sum_{j=1}^{N_d} \sum_{i=1}^n |H_{\text{true}}|^2}}$$

where n is the number of OFDM symbols being transmitted in the simulations and N_d is the number of data sub-carriers within an OFDM symbol. We do a two-dimensional sum over n OFDM symbols and within every OFDM symbol to get a single RMSE value for each case.

These values are tabulated in Table 5.2. These tables give evidence that ESPRIT based method provides the best estimates. But it is also evident that the ESPRIT based method takes the longest time. Execution time for the ESPRIT based method appears to vary by a small amount for different cases. This time difference can be attributed to other applications running on the computer sharing the same processor.

	RMSE	Time (ms)		RMSE	Time (ms)
Linear	0.054	0.228	Linear	0.223	0.246
Cubic spline	0.009	0.233	Cubic spline	0.115	0.213
ESPRIT	0.007	0.878	ESPRIT	0.008	1.068
(a) Delay spread = 2 μ s, $E_b/N_0 = 60$ dB			(b) Delay spread = 4 μ s, $E_b/N_0 = 60$ dB		
	RMSE	Time (ms)		RMSE	Time (ms)
Linear	0.395	0.239	Linear	0.127	0.227
Cubic spline	0.459	0.237	Cubic spline	0.124	0.224
ESPRIT	0.007	1.278	ESPRIT	0.132	1.098
(c) Delay spread = 6 μ s, $E_b/N_0 = 60$ dB			(d) Delay spread = 2 μ s, $E_b/N_0 = 15$ dB		
	RMSE	Time (ms)		RMSE	Time (ms)
Linear	0.208	0.234	Linear	0.363	0.232
Cubic spline	0.151	0.221	Cubic spline	0.430	0.214
ESPRIT	0.123	0.978	ESPRIT	0.124	0.874
(e) Delay spread = 4 μ s, $E_b/N_0 = 15$ dB			(f) Delay spread = 6 μ s, $E_b/N_0 = 15$ dB		

Table 5.2: RMSE and time required for channel estimation

5.1.3 Symbol error rate

For comparison at lower SNR values, Symbol Error Probability (SEP) performance plots for QPSK and 16-QAM modulation schemes for ideal, two-path and three-path channels can be seen in Figures 5.5, 5.6 and 5.7. For reference we have included the theoretical performance curve for an ideal AWGN channel for each case. For an ideal channel, the performance of all three estimation techniques is comparable to each other, as can be seen in Figure 5.5. The comparatively small gap of the curves representing all three techniques to the theoretical curve is attributed to poor estimation in presence of noise.

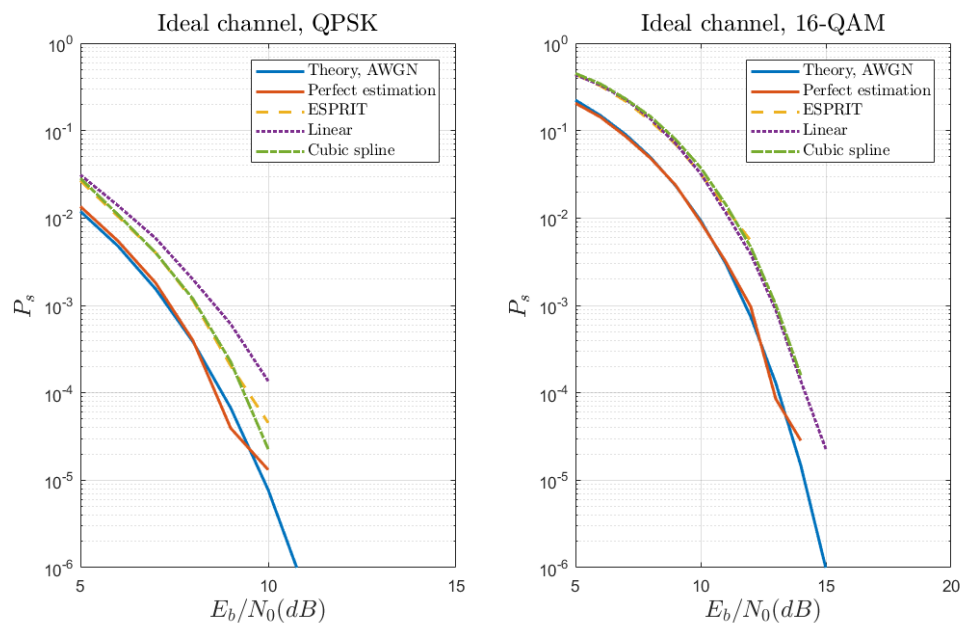


Figure 5.5: Symbol error rate plots for ideal channel

With a delay spread in the system, the gap relative to this reference curve is due to averaging over good and bad subcarriers on the frequency-selective channel. The complex baseband model used for a two-path channel (Figure 5.6) is

$$\tilde{h}(t) = 0.9\delta(t) + 0.5e^{-j\pi/5}\delta(t - 4 \mu s)$$

and that for a three-path channel (Figure 5.7) is

$$\tilde{h}(t) = 0.9\delta(t) + 0.4e^{-j\pi/5}\delta(t - 2 \mu s) + 0.3e^{j\pi/4}\delta(t - 4 \mu s)$$

The maximum delay spread is assumed to be the same in both channel models.

As expected from previous discussion, performance of the ESPRIT-based estimation technique is better than both interpolation techniques; for larger delay spreads the interpolation methods experience error floors as would be inferred from the constellation plots shown before.

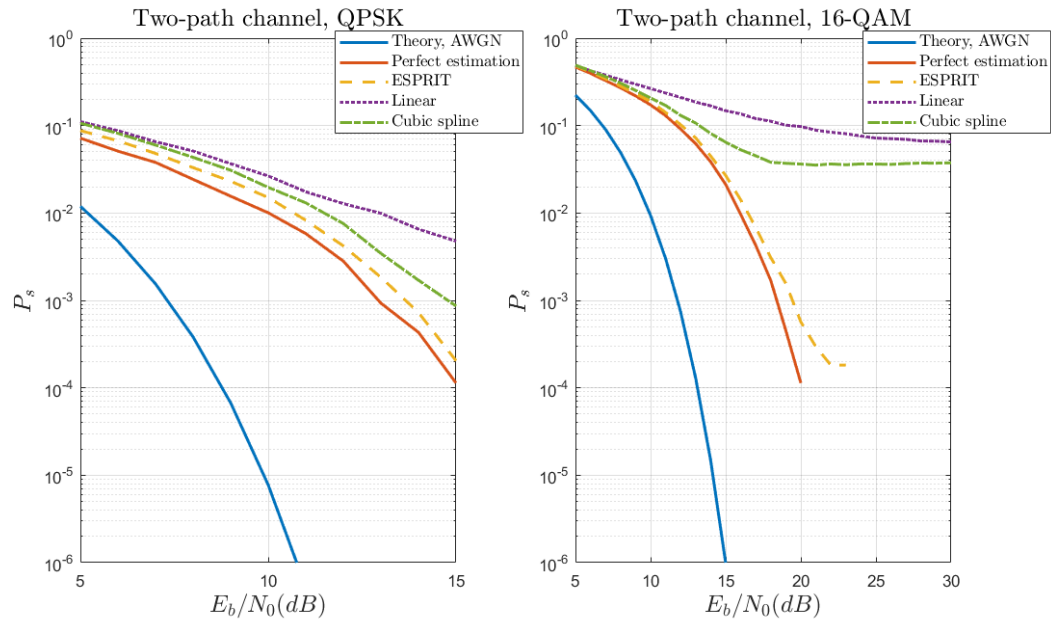


Figure 5.6: Symbol error rate plots for the two-path channel

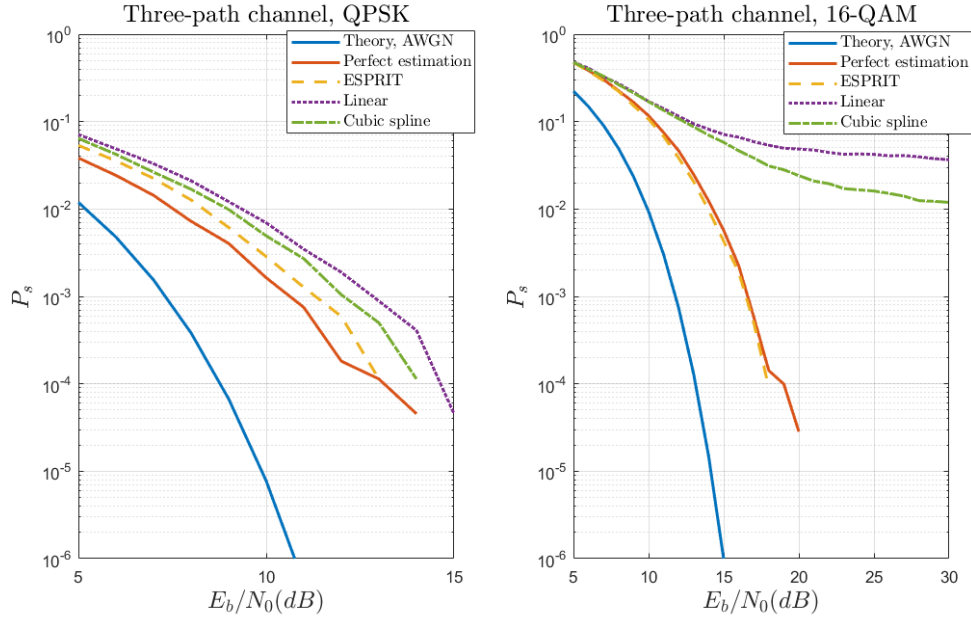


Figure 5.7: Symbol error rate plots for the three-path channel

5.1.4 Shortcomings of ESPRIT-based algorithm

However, the ESPRIT based method does have limitations. In our simulations, the subcarrier spacing is 7.8 kHz, and there are 10 data symbols between consecutive pilot symbols, hence the interval between two pilots is 78 kHz. If we ask this to be greater than or equal to half of the delay spread in the channel, as guided by a sampling theorem, then the largest delay spread the ESPRIT-based method should be able to handle is

$$(\text{Delay spread})_{max} = 1/(2 \times 78000) = 6.4 \mu s$$

Simulations indeed show that for a delay spread of 7 μs , the ESPRIT-based method produces poor constellations as can be seen in Figures 5.8a and 5.8b. The identified channel model is effectively incorrect due to an aliasing effect. In this case, the constellations produced by interpolation techniques are also poor, but better than the ones produced by ESPRIT-based method.

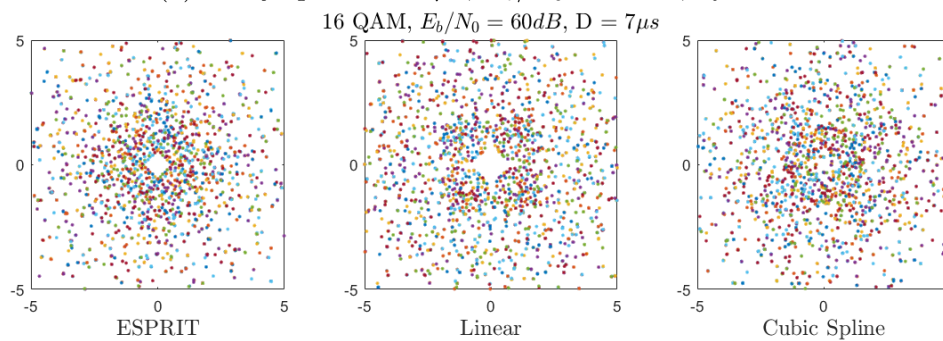
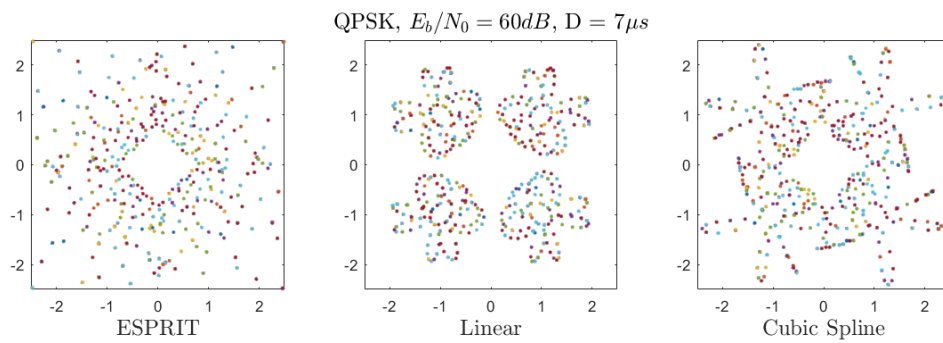


Figure 5.8: Constellations for a delay spread of $7\mu\text{s}$. Left to right: ESPRIT, Linear, Cubic Spline.

Chapter 6

Channel coding

6.1 Motivation

In chapter 3, we have seen that multipath fading in a channel may cause constructive and destructive interference in the CFR. Figure 6.1 shows an example of a 2 path model with noise in the channel. The received signal in the frequency domain is given by

$$Y_{i,n} = X_{i,n}H_{i,n} + N_{i,n}, \quad 1 \leq n \leq N_d$$

Suppose our channel frequency response estimate is $\hat{H}_{i,n}$. When we equalize the received signal with our estimate to recover the transmitted signal (zero-forcing), we get

$$\frac{Y_{i,n}}{\hat{H}_{i,n}} = \frac{X_{i,n}H_{i,n}}{\hat{H}_{i,n}} + \frac{N_{i,n}}{\hat{H}_{i,n}}$$

Around the lowest points in the destructive interference, or the “deep nulls”, the noise $N_{i,n}$ gets divided by a small value (lower than 1) and gets amplified, causing the constellation points of the M-ary QAM modulated symbol to cross decision boundaries and cause errors at the receiver. This is evident from the lower subplot in figure 6.1. Most of the errors in

the system are around these “deep nulls”.

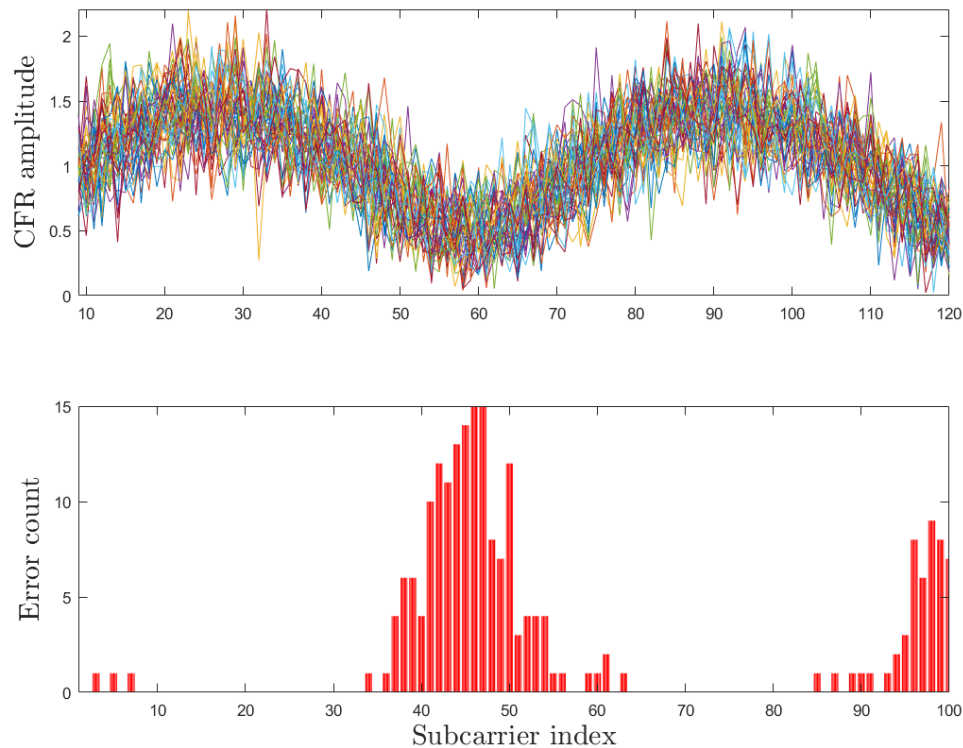


Figure 6.1: Error distribution within OFDM symbols in a 2 path channel with noise.

One solution to compensate for the deep nulls and their corresponding errors is to use channel coding (or forward error correction). Coding across sub-carriers using redundant bits will allow for better system performance against noise, as will be demonstrated below.

6.2 Introduction to channel coding

In any communication system, reliability of the received data through the channel is subject to the level of noise present. Claude Shannon’s coding theorem [14] in 1948 created a general digital communication framework for all communication systems. In this paper,

Shannon defined a new metric called channel capacity (C) which is a measure of how much information a channel can convey. Shannon showed that if the channel code rate R_I (information bits per channel bits) is less than the channel capacity, there exist coding techniques that allow reliable communication. If, $R_I > C$ however, there are no codes that provide reliable communication. Figure 6.2 describes a basic digital communication system that fits into this framework.

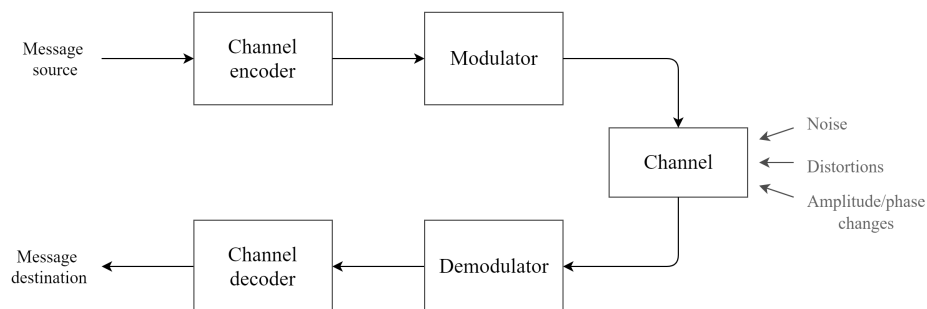


Figure 6.2: Block diagram of a basic digital communication system

Information from the source may be analog (e.g. audio) in form or digital (e.g. computer files). Analog information is converted into digital form before moving on to the next block. This information may also go through source encoders for compression. This thesis pertains mainly to channel coding and does not discuss source coding.

Channel coding is used to protect the input information from channel effects. The channel encoder does so by creating alternate sequences of the information using redundant bits. Using redundancy in coding helps increase the probability of recovering the right information.

The modulator converts the information bits coming from the channel encoder into a form appropriate to be transmitted (OFDM modulation in our case). This signal then is affected by noise, distortions, amplitude and phase changes, etc., in the channel. The demodulator is tasked with converting this received signal back into the information bits from the input of the modulator. These bits are then fed to the channel decoder which attempts to recover the original information from the source. The decoder does so by using either hard-decisions

or soft-decisions.

Hard-decision decoders operate on data that take on a fixed set of possible values (0 or 1 in a binary code). In a soft-decision decoder, the inputs may take on a range of values. This extra information indicates the reliability of each input data point, and is used to form better estimates of the original data. A soft-decision decoder will hence perform better in the presence of noisy data than hard-decision decoder [15].

There are a large number of existing coding techniques and can be divided into two major sets [16]:

- Automatic request-for-repeat (ARQ).
- Forward Error Correction (FEC).

In ARQ schemes, the decoder only detects whether the incoming data packet has errors using very low coding overhead. If even a single error is detected, ARQ schemes will request re-transmission of the same data. ARQ codes are also known as error-detecting codes. These codes cost a setback to the system in terms of delay and throughput.

In FEC techniques, the information is coded by adding redundant bits and using specific algorithms to encrypt the original information. The decoder at the receiver has knowledge of the coding algorithm and can recover the original information even in the presence of (permissible amount of) errors. But due to the added redundant bits, bigger channel bandwidth is required. Hybrid FEC-ARQ techniques also exist which request re-transmission when the receiver fails to correct for the errors in the received information signal.

FEC codes can be divided into two types: *block codes* and *convolutional codes*. Block codes work with packets of information bits or symbols which have a fixed predetermined size. Block codes are often decoded using hard-decisions. Examples of block codes are Hamming codes and Reed-Solomon codes [17]. Convolutional codes on the other hand work with

streams of bits with arbitrary lengths. They are generally decoded by soft-decisions using the Viterbi algorithm.

In this chapter, we focus on block codes known as low-density parity-check (LDPC) codes. LDPC codes were introduced in [18] but went unnoticed for a long time as they were impractical to implement then. But due to the recent advancements in computational power of processors, LDPC codes are gaining importance and popularity in practical applications.

Before discussing LDPC codes, linear block codes are briefly discussed and some important metrics are defined.

Linear block codes

As previously mentioned, data to be coded using block codes is segmented into blocks of fixed length. This length is defined to be K (bits). The encoder then adds redundant bits before implementing the encoding algorithm being used. The output of the encoder is then an encoded block of length N ($N > K$). Each of these blocks is called the codeword. The rate of the code (R) is defined as the ratio of length of un-coded data and the length of coded data, i.e., $R = N/K$.

With K input message bits, 2^K distinct binary input entries are possible. Table look-up encoding would require the encoder to store a table of 2^K entries, each of length N (matrix of size $2^K \times N$). This approach is not practical for large values of K . Linear binary block codes have a property that modulo-2 sum of any two codewords is a codeword. This allows design of a generator matrix (\mathbf{G}) that defines the code. The encoder generates coded symbols using the following formula

$$\mathbf{x} = \mathbf{u}\mathbf{G} \tag{6.1}$$

where \mathbf{u} is the input un-coded data row vector of length K and \mathbf{x} is the output code vector

(codeword) of length N .

\mathbf{G} is made up of K linearly independent row vectors of length N (size of \mathbf{G} is $K \times N$). \mathbf{G} depends on the coding scheme being used and is not unique for a code [17]. This is a significant reduction in size from $2^K \times N$, and using \mathbf{G} allows for an algorithmic approach rather than using table look up..

Another specification necessary to define is the parity-check matrix \mathbf{H} , which spans the null space of the code-space generated by \mathbf{G} . This allows to check for codewords that do not satisfy the coding scheme \mathbf{G} . This gives us a necessary condition

$$\mathbf{x}\mathbf{H}^T = 0, \quad \text{for all codewords} \quad (6.2)$$

where 0 represents a zero vector. Since (6.2) must be satisfied by all codewords spanned by \mathbf{G} , we have

$$\mathbf{G}\mathbf{H}^T = [0]_{K,N-K} \quad (6.3)$$

Thus if one of \mathbf{G} or \mathbf{H} is known, the other can be easily calculated.

6.3 LDPC codes

LDPC codes are a class of linear block codes that are defined by a sparse parity-check matrix \mathbf{H} ; sparseness makes near-ML decoding possible with “message passing” described below. LDPC codes can be generalized to non-binary symbols (in $GF(q)$) but in this thesis, we restrict ourselves to binary codes. Sparsity in the parity-check matrix means the number of 1’s is much less than the number of 0’s in the matrix. The number of 1’s in a row of \mathbf{H} is called as the row-weight k , and the number of 1’s in a column is the column-weight j . The LDPC code is *regular* if j and k are constant.

When \mathbf{H} is full rank, the code rate can be re-written as $R = \frac{K}{N} = \frac{N-M}{N} = 1 - \frac{M}{N}$, where $M = N - K$. The number of 1's in the parity-check matrix is given by Mk or Nj . From $Mk = Nj$, we get $M/N = j/k$. Hence the code rate can be written in terms of row-weights and column-weight as

$$R \geq 1 - \frac{j}{k}$$

The inequality holds for when \mathbf{H} is not full rank [16].

Equation (6.4) represents sparse parity-check matrix for an example case. The Tanner graphs can also be used to represent LDPC codes. Tanner graph for \mathbf{H} in (6.4) is shown in Figure 6.3. Note that the rank of \mathbf{H} here is 4 and thus it is not full rank.

$$H = \begin{bmatrix} 1 & 1 & 1 & 1 & 0 & 0 & 0 & 0 & 0 & 0 \\ 1 & 0 & 0 & 0 & 1 & 1 & 1 & 0 & 0 & 0 \\ 0 & 1 & 0 & 0 & 1 & 0 & 0 & 1 & 1 & 0 \\ 0 & 0 & 1 & 0 & 0 & 1 & 0 & 1 & 0 & 1 \\ 0 & 0 & 0 & 1 & 0 & 0 & 1 & 0 & 1 & 1 \end{bmatrix} \quad (6.4)$$

A Tanner graph is a bipartite graph with two sets of nodes. Nodes in both sets are inter-connected as shown. The two different nodes are named *check nodes* and *variable nodes*. Check nodes and variable nodes represent rows and columns of \mathbf{H} respectively.

The m_c^{th} check node is connected to the n_v^{th} variable node only if $\mathbf{H}_{m_c, n_v} = 1$. The number of edges in each check node is equal to the row weight and the number of edges in each variable node is equal to the column weight. In this example, the row weight is 4 and the column weight is 2.

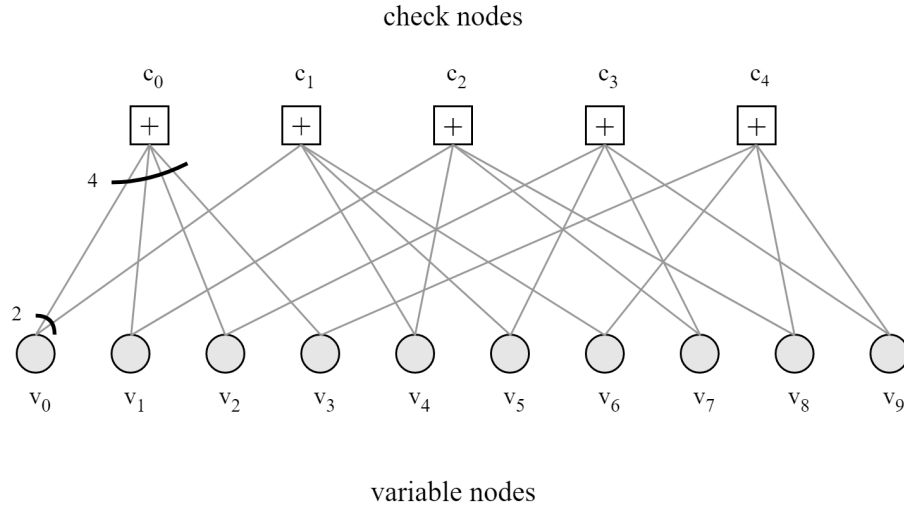


Figure 6.3: Graph representation of LDPC code in (6.4)

6.3.1 LDPC encoding

Encoding of LDPC codes is done similar to other linear block codes discussed earlier in this chapter. From a given parity-check matrix \mathbf{H} , the generator matrix \mathbf{G} is derived. Transmission data $\mathbf{u} = [u_1, u_2, \dots, u_K]$ is encoded by multiplication with \mathbf{G} as in (6.1).

Systematic form of the parity-check matrix can be given by $\mathbf{H} = [P^T \mid I_M]$ where I_M is an identity matrix of size $M \times M$. The computational complexity while encoding depends on the denseness (or sparsity) of P . Quasi-cyclic codes are known to reduce complexity [16]. In quasi-cyclic codes, a cyclic shift by q bits of a codeword results in another.

6.3.2 LDPC decoding

Decoding of LDPC codes is achieved through an iterative process known as message-passing on the Tanner graph. Several message passing algorithms (MPAs) exist that execute this iterative process [16]. These passed messages are probability of confidence estimates.

Specifically, we explore the sum-product algorithm (SPA) [16] for general memory less binary input channels.

The main criteria underlying the development of SPA decoder is symbol-wise maximum *a posteriori* (MAP). Here we are interested in computing the *a posteriori* probability (APP) that the bits in the transmitted symbol $\mathbf{x} = [x_1, x_2, \dots, x_N]$ are equal to 0, given the received word $\mathbf{y} = [y_1, y_2, \dots, y_N]$. The APP is then given by

$$Pr(x_j = 0|\mathbf{y})$$

and the log-likelihood ratio (LLR) is given by

$$L(x_j|\mathbf{y}) = \log_{10} \frac{Pr(x_j = 0|\mathbf{y})}{Pr(x_j = 1|\mathbf{y})} \quad (6.5)$$

The decoding algorithm is usually computed in the log domain to simplify computations and for better numerical stability, as described below.

The Tanner graph has check nodes (CNs) that correspond to the parity constraints and variable nodes (VNs) to represent data bits of the codeword. The MPA estimates codewords by iteratively updating and exchanging messages between connected variable and check nodes on the Tanner graph. All VNs process their inputs and pass extrinsic information to neighboring CNs. Extrinsic information is the one a VN will pass to a CN or vice versa. The CNs then process their inputs and pass extrinsic information to their neighboring VNs. Starting from the VNs, this process repeats. After a predefined number of iterations are completed or some stopping criteria has been met, the decoder produces the final LLRs from which decisions on the bits x_j are made. Increasing the number of iterations will increase the accuracy of decoding the correct bits to a point. One important assumption in SPA is the LLR quantities received at each node from its neighbors are independent [16]

(true only when Tanner graphs are cycle-free).

The extrinsic information from the j^{th} VN to i^{th} CN is given by

$$L_{j \rightarrow i} = L_j + \sum_{i' \in N(j) - i} L_{i' \rightarrow j} \quad (6.6)$$

where $N(j)$ is the set of all neighboring nodes and L_j is calculated from the channel output y_j as

$$L_j = L(x_j | y_j) = \log_{10} \frac{\text{Pr}(x_j = 0 | y_j)}{\text{Pr}(x_j = 1 | y_j)} \quad (6.7)$$

Note the extrinsic message excludes input messages on the same edge. At the end of the iteration cycle, the j^{th} VN will make a decision based on

$$L_j^{\text{total}} = L_j + \sum_{i \in N(j)} L_{i \rightarrow j} \quad (6.8)$$

Likewise, the extrinsic information computed in i^{th} CN is given by [16]

$$L_{i \rightarrow j} = 2 \tanh^{-1} \left(\prod_{j' \in N(i) - j} \tanh\left(\frac{1}{2} L_{j' \rightarrow i}\right) \right) \quad (6.9)$$

Equations (6.6)-(6.9) form the basis of the SPA decoder. Following is a summary of the iterative SPA algorithm.

1. **Initialize.** The decoder is initialized by setting all VN messages $L_{j \rightarrow i}$ equal to L_j in equation (6.7).
2. **CN update.** Compute $L_{i \rightarrow j}$ for each CN using (6.9) and transmit extrinsic information to neighboring VNs.
3. **VN update.** Compute $L_{j \rightarrow i}$ for each VN using (6.6) and transmit extrinsic information to neighboring CNs.

4. **Accumulated LLR.** For each VN compute the accumulated LLR from (6.8).
5. Set \hat{x} , the estimate of the transmitted symbol to be

$$\hat{x} = \begin{cases} 0, & \text{if } L_j^{total} > 0 \\ 1, & \text{otherwise} \end{cases} \quad (6.10)$$

to obtain $\hat{\mathbf{x}}$. If $\hat{\mathbf{x}}\mathbf{H}^T = 0$ or maximum iterations reached, stop the loop; else go back to step 2.

Long LDPC codes can perform very close to the theoretical limit on energy efficiency (channel capacity).

6.4 Simulation results

Figures 6.4 and 6.5 show the bit-error-rate (BER) curves for an ideal AWGN channel and a two-path slow-fading channel respectively. For both cases, we use a quasi-cyclic LDPC code of rate (R) 0.84. The parity-check matrix (\mathbf{H}) used is of dimensions (1024×6400). Here the encoder will produce a long stream of 6400 coded bits, of which $6400 \times 0.84 = 5376$ bits carry data and the rest are redundant bits. As can be seen in Figure 6.4, the BER performance of the code in an AWGN channel is within 1 *dB* of the channel capacity.

For a two-path channel, we discretize the complex baseband response

$$\tilde{h}(t) = 0.9\delta(t) + 0.5e^{-j\pi/5}\delta(t - 2 \mu s)$$

and do the Fourier transform to get amplitudes of the CFR at the data subcarrier locations. We repeat the 100 data carrier coefficients to get a vector of length 6400 and multiply it with the coded data (which is of the same length). This data then goes to the LDPC

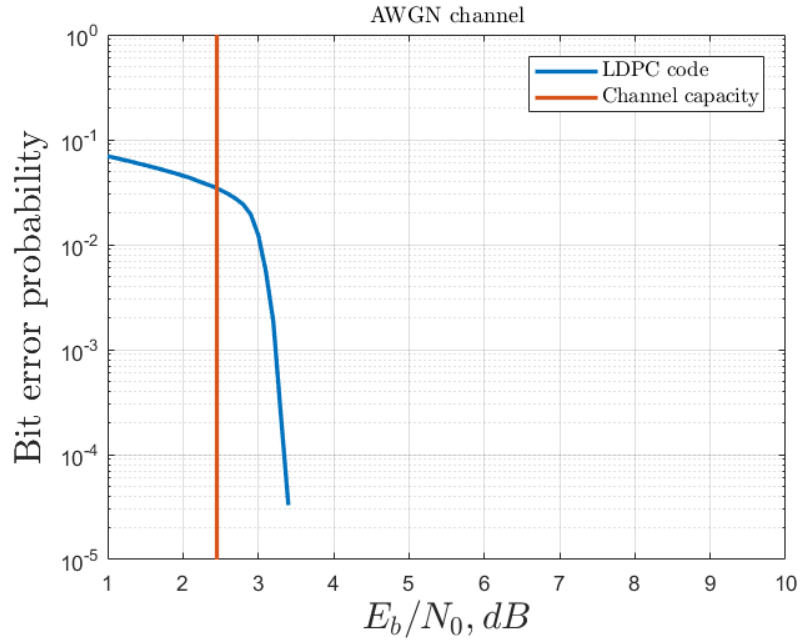


Figure 6.4: BER plot for AWGN channel, $R = 0.84$, $(N, K) = (6400, 5376)$

decoder in the receiver and then the BER calculations are performed.

At P_s (bit-error-probability) = 10^{-4} , we can observe the difference between the curves in Figure 6.4 and Figure 6.5 to be approximately 4dB. This gap is mainly attributed to the fading effects of the two-path channel, and also the imperfection in the PM-based CFR estimation used. Using MMSE compensation in the equalization process will further help improve the BER performance in presence of noise.

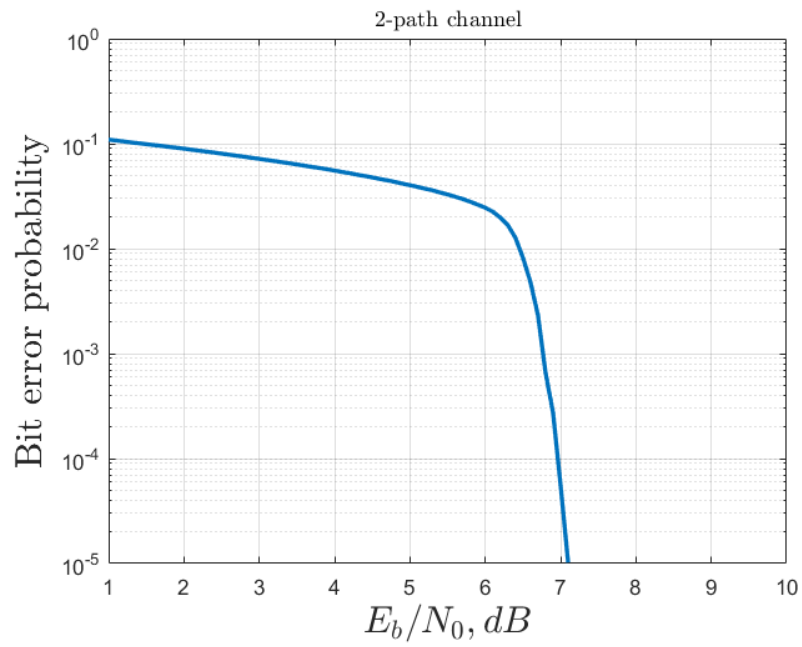


Figure 6.5: BER plot for two-path channel, $R = 0.84$, $(N, K) = (6400, 5376)$

Chapter 7

Conclusion

In this thesis, we evaluate and compare the Symbol Error Probability (SEP) performance of two pilot-aided channel estimation schemes: interpolation and an ESPRIT-based parametric model method. We also look at the time complexity and RMSE values for the estimation techniques. Experimental results suggest that the ESPRIT-based method performs better than the interpolation-based methods. The ESPRIT-based method does have shortcomings, in that it can only handle a delay spread corresponding to less than twice the frequency domain interval between two pilots. Also, depending on the parameter set used, the ESPRIT-based method can be too computationally expensive to be chosen over the interpolation-based methods. We demonstrate the effect of multipath fading in wireless channels on 16 QAM and QPSK modulation schemes using frequency response and constellation plots. We also demonstrate the effect of LDPC channel coding on the BER performance of AWGN and a two-path channel, and show coding gain.

Future work

The ESPRIT-based approach in channel estimation provides decent accuracy in channel estimation but needs uniform pilot distribution and can handle a certain maximum delay

spread in the system. Possible future work is to explore the accuracy of iterative channel estimation techniques and compare them to the techniques presented in this thesis in terms of time-complexity and accuracy.

Another idea of interest is to use frequency interleaving while implementing channel coding (chapter 6), which would shuffle the symbols at all sub-carriers across several code words and create a more uniform distribution of errors compared to the one showed in Figure 6.1. This may help push the BER plots further to the left.

Chapter 8

Bibliography

- [1] S. Haykin and M. Moher. *Modern Wireless Communication*. Prentice-Hall, Inc., Upper Saddle River, NJ, USA, 2004.
- [2] Y. Liu, Z. Tan, H. Hu, L. J. Cimini, and G. Y. Li. Channel estimation for OFDM. *IEEE Communications Surveys Tutorials*, 16(4):1891–1908, Fourthquarter 2014.
- [3] M. A. Deshmukh and S. G. Wilson. Channel estimation in OFDM: Interpolation versus esprit. In *2018 IEEE 8th Annual Computing and Communication Workshop and Conference (CCWC)*, pages 673–678, 2018.
- [4] S. G. Wilson, R. Shang, and R. He. Frame synchronization for OFDM using cyclic prefix and pilot carriers. In *MILCOM 2017 - 2017 IEEE Military Communications Conference (MILCOM)*, pages 214–218, Oct 2017.
- [5] Theodore Rappaport. *Wireless Communications: Principles and Practice*. Prentice Hall PTR, Upper Saddle River, NJ, USA, 2nd edition, 2001.
- [6] J. J. van de Beek, M. Sandell, and P. O. Borjesson. Ml estimation of time and frequency offset in ofdm systems. *IEEE Transactions on Signal Processing*, 45(7):1800–1805, Jul

1997.

- [7] M. K. Ozdemir and H. Arslan. Channel estimation for wireless OFDM systems. *IEEE Communications Surveys Tutorials*, 9(2):18–48, Second 2007.
- [8] Baoguo Yang, K. B. Letaief, R. S. Cheng, and Zhigang Cao. Channel estimation for OFDM transmission in multipath fading channels based on parametric channel modeling. *IEEE Transactions on Communications*, 49(3):467–479, Mar 2001.
- [9] Ye Geoffrey Li, L. J. Cimini, and N. R. Sollenberger. Robust channel estimation for OFDM systems with rapid dispersive fading channels. In *1998 IEEE International Conference on Communications*, volume 3, pages 1320–1324 vol.3, Jun 1998.
- [10] S. Coleri, M. Ergen, A. Puri, and A. Bahai. Channel estimation techniques based on pilot arrangement in OFDM systems. *IEEE Transactions on Broadcasting*, 48(3):223–229, Sep 2002.
- [11] Eric W. Weisstein. Cubic spline. <http://mathworld.wolfram.com/CubicSpline.html>. From MathWorld—A Wolfram Web Resource.
- [12] W. H. Press, S. A. Teukolsky, W. T. Vetterling, and B. P. Flannery. *Numerical Recipes 3rd Edition: The Art of Scientific Computing*. Cambridge University Press, New York, NY, USA, 3 edition, 2007.
- [13] P. Stoica and R.L. Moses. *Introduction to Spectral Analysis*. Prentice Hall, 1997.
- [14] C. E. Shannon. A mathematical theory of communication. *Bell System Technical Journal*, 27(3):379–423, 1948.
- [15] J.G. Proakis. *Digital Communications*. Electrical engineering series. McGraw-Hill, 2001.

- [16] W. Ryan and S. Lin. *Channel Codes: Classical and Modern*. Cambridge University Press, 2009.
- [17] Stephen G. Wilson. *Digital Modulation and Coding*. Prentice-Hall, Inc., Upper Saddle River, NJ, USA, 1996.
- [18] R. Gallager. Low-density parity-check codes. *IRE Transactions on Information Theory*, 8(1):21–28, January 1962.